SMAI-JCM
SMAI Journal of Computational Mathematics

A coupled approach to compute approximate solutions of a compressible immiscible three-phase flow model with fast transient and stiff source terms

Jean-Marc Hérard & Guillaume Jomée

Volume 11 (2025), p. 405-434.
https://doi.org/10.5802/smai-jcm.129

The SMAI Journal of Computational Mathematics is a member of the Centre Mersenne for Open Scientific Publishing
http://www.centre-mersenne.org/
Submissions at https://smai-jcm.centre-mersenne.org/ojs/submission
e-ISSN: 2426-8399

SMAI Journal of Computational Mathematics
Vol. 11, 405-434 (2025)

A coupled approach to compute approximate solutions of a compressible immiscible three-phase flow model with fast transient and stiff source terms

Jean-Marc Hérard [1]
Guillaume Jomée [2]

[1] EDF Lab Chatou, 6 quai Watier, 78400, Chatou, France
E-mail address: jean-marc.herard@edf.fr
[2] EDF Lab Chatou, 6 quai Watier, 78400, Chatou, France
Current address: CEA, CEA Paris-Saclay Center, 91190 Gif-sur-Yvette, France
E-mail address: guillaume.jomee@cea.fr.

Abstract. This paper aims at developing a new numerical coupled approach to compute solutions of a compressible immiscible three-phase flow model with stiff source terms. The targeted applications involve flows with fast transient and shock waves. Thus, a well-posed model with respect to the initial conditions that embarks an entropy inequality is considered. A preliminary work on the underlying relaxation process of the model is conducted. Then the new numerical scheme is presented and numerically tested.

2020 Mathematics Subject Classification. 76T30, 65M08, 34C26.

Keywords. Multiphase flows, Hyperbolic Systems, Relaxation, Compressible fluids, Transient flows, Steam explosion.

Introduction

This work tackles the simulation of steam explosions, which involve unsteady patterns including sudden heat and mass exchanges between phases, and also shock waves. In our applications, steam explosion occurs when a very high temperature liquid metal, called corium, meets liquid water (see [5]). The contact between liquid water and corium vaporizes the liquid water into water vapour, and leads to the fragmentation of the corium droplets into smaller ones, which accelerates the energy exchange between the liquid metal and the water, and thus leads to an explosion. The fragmentation of droplets is driven by relative velocities between liquid metal droplets and the water, see [25]. Thus, it is mandatory in our applications that the considered model can take into account relative velocities. Therefore, we need a compressible, three-phase flow model that includes heat and mass transfer, and relative velocities. Hence, for our applications, the following specifications are necessary:

(C1) an entropy inequality holds for smooth solutions of the whole model,

(C2) shock relations are uniquely defined,

(C3) the model is at least hyperbolic or even symmetrisable so that the problem becomes well posed with respect to initial conditions [43].

The model chosen for this work is the one introduced in [30]. This model can be seen as an extension to the three-phase flow framework of the more classical Baer–Nunziato model [3] used in the two-phase

This work has been achieved during the PhD thesis of the second author at EDF Lab Chatou and Aix-Marseille University, with partial financial support from ANRT under EDF-CIFRE contract number 2020-0946.
https://doi.org/10.5802/smai-jcm.129

flow framework (see [37] for a formal derivation). It must be emphasized that an extension of this model to an undetermined number of phases has been proposed in [47].

Different numerical strategies exist in the literature for tackling hyperbolic models with stiff source terms (see the review presented in [7]). Focusing on the two-phase flow framework, and more precisely the Baer–Nunziato model, the literature regarding the simulation of this model mainly focuses on the numerical treatment of the convective part of the model (which corresponds to zero source terms) see for example [16, 56, 57, 58]. When the full model is considered (with non-zero source terms), the numerical strategy mainly used up to now consists in computing first solutions of the convective part of the model with an explicit solver, and then accounting for the ODE part of the model (source terms) using an implicit method. In practice, the source terms are mainly treated with a fractional step method, that treats successively the four relaxation processes (see among others [1, 17, 22, 33, 48, 49]). However, as exhibited in [35], this method can have some stability issues when dealing with the full model, including heat and mass transfer and velocity and pressure relaxation. Indeed, the full Baer–Nunziato model embarks a complex set of source terms which creates a stiff non-linear system that can be uneasy to solve. In [35], a more coupled strategy for treating the source terms, based on a better understanding of the underlying ODE system is presented. It actually gives better results on coarse grids and it enables to compute some cases where the fractional step approach fails. A somewhat similar strategy has also been presented in [14], for the Baer–Nunziato model without heat and mass transfer.

Coming back to the three-phase flow framework, a first attempt to tackle steam explosion with the model [30] has been carried out in [9]. However, the numerical schemes proposed in [9] occurred not to be stable enough to compute numerical approximation of solutions of the full model. For steam explosions, some assumptions on instantaneous equilibrium between phases were indeed mandatory to compute numerical solutions. However, those assumptions (and especially the velocity equilibrium) were too strong and inhibited the fragmentation of liquid metal droplets. As a consequence, the maximum pressure values were two times smaller than the ones measured in [39].

Hence, as in the two-phase flow framework, taking into account the immiscible three-phase flow model [30] is challenging, since twelve relaxation time scales associated with pressure, velocity, temperature, Gibbs relaxation are introduced in model [30], and drive the solutions.

Going further on into details, each of those relaxation time scales spans a large interval. Moreover, there is no systematic ordering of those time scales, and their values change drastically with respect to time and space, mainly due to their conditioning by the statistical fractions and thermodynamic coefficients (see Appendix B). Those time scales, associated with the source terms of the model, generate a stiff non-linear coupled ODE's system. In this paper we want to extend the method proposed in [35] for the treatment of source terms of a two-phase flow model [3] to the considered three-phase flow model [30].

The paper is organized as follows. The full model, including all closure laws, is first recalled in Section 1, together with its main properties. Then, focus is given in Section 2 on the effective relaxation process associated with source terms. Afterwards, Section 3 will detail the numerical approach which relies on a two-step explicit/implicit method, where the convective part of the model is estimated first, using an explicit scheme, while the second step takes all source terms into account in a linear-implicit way. The explicit strategy in Step 1 enables to define a time step which in some sense guarantees an optimal accuracy of fast waves. The linear-implicit algorithm proposed in Step 2 is derived from the analysis conducted in Section 2, and its properties are given. This linear-implicit strategy is therefore specific to model [30]. The last Section provides results of some numerical experiments, including a numerical study of convergence with respect to the mesh size.

1. **The immiscible three-phase flow model** [30]

We consider an immiscible, compressible, non-equilibrium, three-phase flow model. In the application Section 4, phase 1 will correspond to a liquid metal, phase 2 to liquid water and phase 3 to water vapour. First, as the model is assumed to be immiscible, we have the structural constraint:

$$\alpha_1 + \alpha_2 + \alpha_3 = 1 \ . \tag{1.1}$$

where $\forall\ k \in [\![1,3]\!]$, $\alpha_k \in]0,1[$ denote the statistical fractions of each phase. Moreover, since the model is in full disequilibrium, each phase k $\in [\![1,3]\!]$ is given a velocity U_k, a density ρ_k, a partial density $m_k = \alpha_k \rho_k$, a pressure P_k and a specific entropy s_k. The total energies are then defined as:

$$E_k = \rho_k(\epsilon_k(P_k,\rho_k) + U_k^2/2), \tag{1.2}$$

where $\epsilon_k(P_k,\rho_k)$ denotes the internal energy of each phase k. The internal energy of phase k is related to the pressure P_k and density ρ_k through an Equation of State (EoS). The vector of state variables W reads:

$$W = (\alpha_2, \alpha_3, m_1, m_1U_1, \alpha_1E_1, m_2, m_2U_2, \alpha_2E_2, m_3, m_3U_3, \alpha_3E_3)^\intercal \ . \tag{1.3}$$

Then, the model reads (see [30]):

$$\begin{cases} \dfrac{\partial \alpha_k}{\partial t} + \mathcal{V}_I(W)\cdot\nabla\alpha_k = S_k^\alpha(W) \ , \\ \dfrac{\partial m_k}{\partial t} + \nabla\cdot(m_kU_k) = S_k^m(W) \ , \\ \dfrac{\partial m_kU_k}{\partial t} + \nabla\cdot(m_kU_k\otimes U_k + \alpha_kP_k\mathcal{I}) + \displaystyle\sum_{l=1,l\neq k}^{3} \Pi_{kl}(W)\nabla\alpha_l = S_k^U(W) \ , \\ \dfrac{\partial \alpha_kE_k}{\partial t} + \nabla\cdot(\alpha_kU_k(E_k+P_k)) - \displaystyle\sum_{l=1,l\neq k}^{3} \Pi_{kl}(W)\frac{\partial\alpha_l}{\partial t} = S_k^E(W) \ , \end{cases} \tag{1.4}$$

where $\mathcal{I}$ is the identity matrix. Moreover, $\mathcal{V}_I$ and Π_{kl} respectively stand for the interfacial velocity and the interfacial pressures. Those interfacial terms, alongside source terms $S_k^\alpha(W)$, $S_k^m(W)$, $S_k^U(W)$ and $S_k^E(W)$, have to be specified in order to close the model. To do so, the total entropy $\eta(W)$ paired with its entropy-flux $\mathcal{F}_\eta(W)$, are introduced:

$$\begin{cases} \eta = m_1s_1(P_1,\rho_1) + m_2s_2(P_2,\rho_2) + m_3s_3(P_3,\rho_3) \ , \\ \mathcal{F}_\eta = m_1U_1s_1(P_1,\rho_1) + m_2U_2s_2(P_2,\rho_2) + m_3U_3s_3(P_3,\rho_3) \ . \end{cases} \tag{1.5}$$

Definitions of the phasic temperature T_k, the phasic Gibbs free energy μ_k, the phasic enthalpy h_k and the phasic speed of sound c_k are also recalled:

$$\frac{1}{T_k} = \frac{\partial_{P_k}\left(s_k(P_k,\rho_k)\right)|_{\rho_k}}{\partial_{P_k}\left(\epsilon_k(P_k,\rho_k)\right)|_{\rho_k}} \tag{1.6}$$

$$\mu_k = h_k - T_kS_k \tag{1.7}$$

$$h_k = \epsilon_k(P_k,\rho_k) + \frac{P_k}{\rho_k} \tag{1.8}$$

$$c_k^2\ \partial_{P_k}\left(s_k(P_k,\rho_k)\right)|_{\rho_k} + \partial_{\rho_k}\left(s_k(P_k,\rho_k)\right)|_{P_k} = 0 \tag{1.9}$$

The strategy for closing the model is to ensure that it respects the following mathematical properties: hyperbolicity of the convective part (i.e. supposing $S_k^\alpha = S_k^m = S_k^U = S_k^E = 0$.) (C3), uniqueness of jump relations (C2), and compliance with an entropy inequality for the mixture for smooth solutions of the model (C1).

We briefly recall now the modeling strategy introduced in [30], which is grounded on the one introduced for the two-phase flow framework in [15]. First of all, the following form of the interfacial velocity $\mathcal{V}_I$ is assumed, as a convex combination of phasic velocities U_k:

$$\mathcal{V}_I(W) = \sum_k \beta_k(W) U_k \tag{1.10}$$

(where W stands for the state variable and the $\beta_k(W)$ are positive functions that remain to be prescribed), which is a priori meaningful since it is Galilean invariant when: $\sum_k \beta_k(W) = 1$. This form is also expected from a phenomenological point of view.

Then, the entropy inequality for the mixture (C1) enables to exhibit a *unique set of interfacial pressures* $\Pi_{k,l}$, which only depend on the $\beta_k(W)$ (see Appendix G in [30]).

Enforcing the entropy inequality (C1) allows to propose a class of admissible source terms $S(W)$ (depending on the local state variable W). The latter source terms require physically relevant relaxation time scales, to be found in the two-phase flow literature.

Eventually, it only remains to propose a suitable form of functions $\beta_k(W)$ in order to comply with condition (C2).

In the general case, jump conditions are not uniquely defined when some non-conservative products occur (see for instance [18] for an introduction to hyperbolic systems without conservative form). It is for example the case for turbulent compressible models using second-moment closures see [2] and [4]. However, in certain cases, field by field jump conditions may be uniquely defined when non-conservative products are not active in Genuinely Non Linear (GNL) fields.

Focusing first on the two-phase flow framework and Baer–Nunziato like models, the interfacial velocity $\mathcal{V}_I$ remains to be defined. Enforcing the Linearly Degenerate (LD) structure for the field associated with the eigenvalue $\lambda = \mathcal{V}_I$ ensures that the non-conservative products are well defined through each field. This was discussed in [15] and later on in [29] (for the barotropic case). Moreover, if the choice of $\mathcal{V}_I$ does not comply with the LD structure for $\lambda = \mathcal{V}_I$, jump conditions may be no longer unique (see [28, Figure 8.3 p. 136] for numerical drawbacks). Suitable forms for $\beta_k(W)$ are:

$$\beta_k(W) = \frac{d_k \alpha_k \rho_k}{\sum_{l=1}^2 d_l \alpha_l \rho_l} \tag{1.11}$$

with $\sum_{k=1}^2 d_k = 1$ and $d_1 \in \{0, 1/2, 1\}$, see [15]. [28] extends this to $d_1 \in [0, 1]$, with d_1 constant. More complex possibilities are given in [31].

This extends to the three-phase flow framework. For model [30], the corresponding suitable forms are [34]:

$$\mathcal{V}_I = U_k \tag{1.12}$$

for $k \in \{1, 2, 3\}$, or:

$$\mathcal{V}_I = \frac{\sum_{k=1}^3 m_k U_k}{\sum_{k=1}^3 m_k} \tag{1.13}$$

In the sequel we choose:

$$\mathcal{V}_I = U_1 \tag{1.14}$$

in order to compare results with [9]. This choice of interfacial velocity is also motivated by the fact that, in our applications, phase 1 corresponds to the dispersed phase, following the former idea of [3].

The choice (1.14) leads to the following *unique* interfacial pressure definition, owing to the entropy inequality (see Appendix G in [30]):

$$\begin{cases} \Pi_{12} = \Pi_{21} = \Pi_{23} = P_2 \ , \\ \Pi_{13} = \Pi_{31} = \Pi_{32} = P_3. \end{cases} \tag{1.15}$$

Before closing the source terms, let us recall some properties of the convective part of the model in a one dimensional framework.

Reminding that system (1.4) is invariant under frame rotation, we introduce a unit vector $\vec{n}$ in $\mathbb{R}^3$ and define $x_n = x \cdot n$ n for $k \in [\![1,3]\!]$:

$$w_k = U_k \cdot n \tag{1.16}$$

$$f_\eta = \mathcal{F}_\eta \cdot n \tag{1.17}$$

Getting rid of transverse variations and considering zero source terms, we end up with the following system in the *one dimensional framework*:

$$\begin{cases} \dfrac{\partial \alpha_k}{\partial t} + w_1 \partial_{x_n} \alpha_k = 0 \ , \\ \dfrac{\partial m_k}{\partial t} + \partial_{x_n}(m_k w_k) = 0 \ , \\ \dfrac{\partial m_k w_k}{\partial t} + \partial_{x_n}(m_k \ w_k^2 + \alpha_k P_k) + \displaystyle\sum_{l=1, l\neq k}^{3} \Pi_{kl}(W) \partial_{x_n} \alpha_l = 0 \ , \\ \dfrac{\partial \alpha_k E_k}{\partial t} + \partial_{x_n}\left(\alpha_k w_k (E_k + P_k)\right) - \displaystyle\sum_{l=1, l\neq k}^{3} \Pi_{kl}(W) \frac{\partial \alpha_l}{\partial t} = 0 \ . \end{cases} \tag{1.18}$$

Then, according to [30, 32], this sub-system has the following property:

Property 1 (Convective part of the three-phase flow model in a 1D framework)**.** *If* $\forall\ k \in [\![1,3]\!], \alpha_k$ *stay in* $]0,1[$ *and* $|w_k - w_1| \neq c_k$*, then:*

- *System* (1.18) *is symmetrizable and its associated eigenvalues are:*

$$\begin{aligned} &\lambda_{1,2,3}(W,n) = w_1, \qquad \lambda_4(W,n) = w_2, \qquad \lambda_5(W,n) = w_3, \\ &\lambda_{6,7}(W,n) = w_1 \pm c_1, \quad \lambda_{8,9}(W,n) = w_2 \pm c_2, \quad \lambda_{10,11}(W,n) = w_3 \pm c_3 \ . \end{aligned} \tag{1.19}$$

- *Fields associated with* λ_k $(k = 6-11)$ *are GNL. Other fields are LD. Riemann invariants within each wave can be found in* [30, Appendices B and E]*.*

- *Jump relations associated with system* (1.18) *are unique (see* [30, Appendix C]*).*

- *Smooth solutions of* (1.18) *satisfy:*

$$\partial_t \eta + \partial_{x_n} f_\eta = 0 \tag{1.20}$$

Property 1 can be extended to a three-dimensional framework, see [30] and [9].

Remark 1.1. In our nuclear applications, condition $|w_k - w_1| \neq c_k$ is always checked in each cell and at each time step, and it has never been violated yet. However, there is no theoretical proof that ensures that it could never happen, even in the one-dimensional two-phase flow framework.

Then, coming back to the three-dimensional framework and therefore system (1.4), source terms have to be closed. The strategy for closing those terms is to select a form so that smooth solutions of system (1.4) comply with the entropy inequality:

$$\partial_t \eta + \nabla \cdot \mathcal{F}_\eta \geq 0. \tag{1.21}$$

We define V_{kl} and H_{kl} as:

$$V_{kl} = \frac{U_k + U_l}{2} \ , \tag{1.22}$$

$$H_{kl} = \frac{U_k \cdot U_l}{2} \ . \tag{1.23}$$

It may be checked that the following closure laws for drag effects, mass transfer, heat transfer and pressure relaxation:

$\forall\, k \in [\![1,3]\!]$:

$$S_k^{\alpha} = \sum_{l=1,l\neq k}^{3} K_{kl}(W)(P_k - P_l) \ , \tag{1.24}$$

$$S_k^{m} = \sum_{l=1,l\neq k}^{3} \Lambda_{kl}(W)\left(\frac{\mu_l}{T_l} - \frac{\mu_k}{T_k}\right) \ , \tag{1.25}$$

$$S_k^{U} = \sum_{l=1,l\neq k}^{3} d_{kl}(W)(U_l - U_k) + \sum_{l=1,l\neq k}^{3} V_{kl}\Lambda_{kl}(W)\left(\frac{\mu_l}{T_l} - \frac{\mu_k}{T_k}\right) \ , \tag{1.26}$$

$$S_k^{E} = \sum_{l=1,l\neq k}^{3} q_{kl}(W)(T_l - T_k) + \sum_{l=1,l\neq k}^{3} V_{kl}\cdot(U_l - U_k)d_{kl}(W) + \sum_{l=1,l\neq k}^{3} H_{kl}\Lambda_{kl}(W)\left(\frac{\mu_l}{T_l} - \frac{\mu_k}{T_k}\right), \tag{1.27}$$

comply with inequality (1.21). These closures are the straightforward counterpart of two-phase closure laws.

Considering strictly positive α_k values, the strictly positive functions $K_{kl}(W)$, $\Lambda_{kl}(W)$, $d_{kl}(W)$ and $q_{kl}(W)$ are defined as:

$$K_{kl}(W) = \frac{\alpha_k\alpha_l}{\mathcal{P}_0\tau_{kl}^{P}(W)} \ , \tag{1.28}$$

$$\Lambda_{kl}(W) = \frac{m_k m_l}{(m_k+m_l)\Gamma_0\tau_{kl}^{m}(W)} \ , \tag{1.29}$$

$$d_{kl}(W) = \frac{m_k m_l}{(m_k+m_l)\tau_{kl}^{U}(W)} \ , \tag{1.30}$$

$$q_{kl}(W) = \frac{m_k m_l C_{v_k} C_{v_l}}{(m_k C_{v_k} + m_l C_{v_l})\tau_{kl}^{T}(W)} \ . \tag{1.31}$$

Quantities C_{V_k} denote the specific heat capacities at constant volume. $\mathcal{P}_0$ is a positive reference pressure, Γ_0 is a positive reference fraction of $\frac{\mu}{T}$.

For each phasic connection $k-l$, $\tau_{kl}^{P}(W)$, $\tau_{kl}^{m}(W)$, $\tau_{kl}^{T}(W)$ and $\tau_{kl}^{U}(W)$ are the symmetric strictly positive relaxation time scales related to the return to equilibrium of the associated thermodynamic quantity between phase k and l. Closure laws for the relaxation time scales can be found in the two-phase flow literature, see among others [10, 23] for the pressure, [40] for the velocity, [54] for the temperature and [6] for mass transfer.

No assumption about these *strictly* positive time scales is imposed, either when studying the overall relaxation process, or when constructing the numerical scheme for processing the source terms.

The previous closing strategy is detailed in [30] and has been used for other multiphase flow models, see among others [15, 34, 38, 53] for two-phase and three-phase flow models. Other closure strategies for the two-phase flow framework exist in the literature, see among others : [19, 24, 26, 42, 47, 50].

Restricting to our application framework -steam explosion-, where phase 1 is supposed to be a liquid metal, no phase change between phase 1 and phase 2 (liquid water) or 3 (water vapour) can occur physically, which implies:

$$\Lambda_{12}(W) = \Lambda_{13}(W) = 0 \ . \tag{1.32}$$

Moreover, we define:

$$\forall\, k \in [\![1,3]\!], \quad g_k = \frac{\mu_k}{T_k} \ . \tag{1.33}$$

Then, we suppose in Section 2 the following:

$$\forall\, k \in [\![1,3]\!]\ ,\ \forall\, \Psi \in \{\alpha_k, P_k, U_k, m_k U_k, \alpha_k E_k\}\ ,\quad \nabla \Psi = 0\ , \tag{1.34}$$

and we set:

$$\forall\, (k,l) \in [\![1,3]\!]^2\ ,\ \forall\, \Phi_k \in \{U_k, P_k, T_k, g_k\}\ ,\quad \Delta\Phi_{kl} = \Phi_k - \Phi_l. \tag{1.35}$$

2. **Relaxation process in the model**

In the sequel, the emphasis will be on the notion of effective relaxation defined as follows.

Consider a system of ODEs:

$$\frac{dY}{dt} = -RY, \tag{2.1}$$

where Y is in $\mathbb{R}^n$ and R an invertible matrix in $\mathcal{M}_n(\mathbb{R})$. If the real parts of all eigenvalues of matrix R remain positive, then the relaxation of system (2.1) will be said to be effective.

The aim of this Section is to give conditions that stand true when the relaxation is effective.

Owing to (1.34) and (1.32) system (1.4) reduces to an ODE system:

$$\begin{cases} \dfrac{\partial \alpha_k}{\partial t} = \displaystyle\sum_{l=1, l\neq k}^{3} K_{kl}(W)\Delta P_{kl}\ , \\ \dfrac{\partial m_k}{\partial t} = -\displaystyle\sum_{l=1, l\neq k}^{3} \Lambda_{kl}(W)\Delta g_{kl}\ , \\ \dfrac{\partial m_k U_k}{\partial t} = -\displaystyle\sum_{l=1, l\neq k}^{3} d_{kl}(W)\Delta U_{kl} - \sum_{l=1, l\neq k}^{3} V_{kl}\Lambda_{kl}(W)\Delta g_{kl}\ , \\ \dfrac{\partial \alpha_k E_k}{\partial t} - \displaystyle\sum_{l=1, l\neq k}^{3} \Pi_{kl}(W)\frac{\partial \alpha_l}{\partial t} \\ \qquad\qquad = -\displaystyle\sum_{l=1, l\neq k}^{3} q_{kl}(W)\Delta T_{kl} - \sum_{l=1, l\neq k}^{3} V_{kl} d_{kl}(W)\Delta U_{kl} - \sum_{l=1, l\neq k}^{3} H_{kl}\Lambda_{kl}(W)\Delta g_{kl}\ . \end{cases} \tag{2.2}$$

Considering hypothesis (1.32), and using the definition of V_{kl}, of H_{kl}, of the sound speed c_k and of the Gibbs free energy μ_k, then, for each phase $k \in [\![1,3]\!]$, equations of evolution of velocity U_k, pressure P_k, temperature T_k and fraction g_k can be derived from system (2.2). Therefore, governing equations of the gaps: $\Delta U_{12}, \Delta U_{13}, \Delta P_{12}, \Delta P_{13}, \Delta T_{12}, \Delta T_{13}, \Delta g_{23}$ can be obtained. Those equations can be rewritten as one equation of evolution of the quantity:

$$\Delta^r = (\Delta U_{12}, \Delta U_{13}, \Delta P_{12}, \Delta P_{13}, \Delta T_{12}, \Delta T_{13}, \Delta g_{23})^\intercal\ \in \mathbb{R}^7\ . \tag{2.3}$$

The equation of evolution associated with Δ^r reads as:

$$\partial_t\left(\Delta^r\right) = -\mathcal{R}^{relax}(W)\Delta^r\ , \tag{2.4}$$

where the non symmetric matrix $\mathcal{R}^{relax}$ in $\mathcal{M}_7(\mathbb{R})$ takes the form:

$$\mathcal{R}^{relax} = \begin{pmatrix} R_{UU} & 0 \\ R_U & \mathcal{R}_{thermo} \end{pmatrix}, \tag{2.5}$$

where $R_{UU} \in \mathcal{M}_2(\mathbb{R})$, $\mathcal{R}_{thermo} \in \mathcal{M}_5(\mathbb{R})$ and $R_U \in \mathcal{M}_{5,2}(\mathbb{R})$.

All coefficients of $\mathcal{R}^{relax}$ can be found in Appendix B.

The velocity relaxation process has a peculiar role in the global relaxation process. A similar result has been found in the framework of a two-phase flow model, see [35].

Alongside equation (2.4), when considering hypothesis (1.32) and (1.34), the following conservation laws can be deduced from system (2.2):

$$\partial_t (m_1) = 0 \tag{2.6}$$
$$\partial_t (m_2 + m_3) = 0 \tag{2.7}$$
$$\partial_t (m_1 U_1 + m_2 U_2 + m_3 U_3) = 0 \tag{2.8}$$
$$\partial_t (\alpha_1 E_1 + \alpha_2 E_2 + \alpha_3 E_3) = 0 \tag{2.9}$$

Hence, we have four stationary constraints (2.6), (2.7), (2.8), (2.9), plus seven unsteady equations embedded in (2.4).

From equation (2.4), effective relaxation conditions can be obtained for model (1.4).

Property 2 (Necessary conditions for effective relaxation of the three-phase flow model)**.**

- *The velocity relaxation process occurs when and only when the non-symmetric velocity relaxation matrix is positive definite:*

$$\mathrm{tr}(R_{UU}) > 0 \ , \tag{2.10}$$
$$\det(R_{UU}) > 0 \ . \tag{2.11}$$

- *We note, for $i \in [\![1, 5]\!]$, λ_i the real or complex conjugate eigenvalues of $\mathcal{R}_{thermo}$. If the thermodynamic relaxation process is effective, then we have:*

$$\Sigma_1 = \mathrm{tr}(\mathcal{R}_{thermo}) > 0 \ , \tag{2.12}$$
$$\Sigma_2 = \sum_{i<j} \lambda_i \lambda_j > 0 \ , \tag{2.13}$$
$$\Sigma_3 = \sum_{i<j<k} \lambda_i \lambda_j \lambda_k > 0 \ , \tag{2.14}$$
$$\Sigma_4 = \sum_{i<j<k<l} \lambda_i \lambda_j \lambda_k \lambda_l > 0 \ , \tag{2.15}$$
$$\Sigma_5 = \det(\mathcal{R}_{thermo}) > 0 \ , \tag{2.16}$$

Proof. The proof reads as follows:
First item of Property 2:

(i) if the velocity relaxation occurs, then the real parts of the two eigenvalues l_1 and l_2 of matrix R_{UU} are strictly positive. Then, the two conditions (2.10) and (2.11) are easily verified.

(ii) Moreover, if conditions (2.10) and (2.11) are verified, it is trivial that both real parts of l_1 and l_2 are positive.

Besides, if mass transfer between phase 2 and 3 is neglected, i.e. $\Lambda_{23} = 0$, conditions (2.10) and (2.11) always stand true, since $d_{kl} > 0$ and $\mathrm{tr}(R_{UU})$ and $\det(R_{UU})$ read:

$$\mathrm{tr}(R_{UU}) = \frac{1}{m_1}(d_{12} + d_{13}) + \frac{1}{m_2}(d_{12} + d_{23}) + \frac{1}{m_3}(d_{13} + d_{23}) > 0$$
$$\det(R_{UU}) = \left[\frac{1}{m_1 m_2} + \frac{1}{m_1 m_3} + \frac{1}{m_2 m_3}\right](d_{12}d_{13} + d_{12}d_{23} + d_{13}d_{23}) > 0$$

If the thermodynamic relaxation process is effective, then the real part of the five eigenvalues of $\mathcal{R}_{thermo}$, $\lambda_i,\ i \in [\![1,5]\!]$ is positive. The five coefficients Σ_1, Σ_2, Σ_3, Σ_4 and Σ_5 write:

$$\begin{aligned}
\Sigma_1 &= \lambda_1+\lambda_2+\lambda_3+\lambda_4+\lambda_5 \ , \\
\Sigma_2 &= \lambda_1\lambda_2+\lambda_1\lambda_3+\lambda_1\lambda_4+\lambda_1\lambda_5+\lambda_2\lambda_3+\lambda_2\lambda_4+\lambda_2\lambda_5+\lambda_3\lambda_4+\lambda_3\lambda_5+\lambda_4\lambda_5 \ , \\
\Sigma_3 &= \lambda_1\lambda_2\lambda_3+\lambda_1\lambda_2\lambda_4+\lambda_1\lambda_2\lambda_5+\lambda_1\lambda_3\lambda_4+\lambda_1\lambda_3\lambda_5+\lambda_1\lambda_4\lambda_5+\lambda_2\lambda_3\lambda_4+\lambda_2\lambda_3\lambda_5 \\
&\qquad +\lambda_2\lambda_4\lambda_5+\lambda_3\lambda_4\lambda_5 \ , \\
\Sigma_4 &= \lambda_2\lambda_3\lambda_4\lambda_5+\lambda_1\lambda_3\lambda_4\lambda_5+\lambda_1\lambda_2\lambda_4\lambda_5+\lambda_1\lambda_2\lambda_3\lambda_5+\lambda_1\lambda_2\lambda_3\lambda_4 \ , \\
\Sigma_5 &= \lambda_1\lambda_2\lambda_3\lambda_4\lambda_5 \ .
\end{aligned}$$

As $\mathcal{R}_{thermo}$ lies in $\mathcal{M}_5(\mathbb{R})$, three cases can occur:

Case 1. All of the eigenvalues of $\mathcal{R}_{thermo}$ are real. Then, if all eigenvalues of $\mathcal{R}_{thermo}$ are positive, all coefficients $\Sigma_n,\ n \in [\![1,5]\!]$ are trivially positive.

Case 2. One eigenvalue of $\mathcal{R}_{thermo}$ is real (let's call it λ_1) and the other four are complex and form two pairs of complex conjugate ($\lambda_3 = \overline{\lambda_2}$ and $\lambda_5 = \overline{\lambda_4}$). Thus, coefficients $\Sigma_n,\ n \in [\![1,5]\!]$ write as:

$$\Sigma_1 = \lambda_1 + 2\mathfrak{Re}(\lambda_2) + 2\mathfrak{Re}(\lambda_4) \ , \tag{2.17}$$

$$\Sigma_2 = 2\lambda_1\mathfrak{Re}(\lambda_2) + 2\lambda_1\mathfrak{Re}(\lambda_4) + 4\mathfrak{Re}(\lambda_2)\mathfrak{Re}(\lambda_4) + |\lambda_2|^2 + |\lambda_4|^2 \ , \tag{2.18}$$

$$\Sigma_3 = \lambda_1\left(|\lambda_2|^2 + |\lambda_4|^2\right) + 4\lambda_1\mathfrak{Re}(\lambda_2)\mathfrak{Re}(\lambda_4) + 2|\lambda_2|^2\mathfrak{Re}(\lambda_4) + 2|\lambda_4|^2\mathfrak{Re}(\lambda_2) \ , \tag{2.19}$$

$$\Sigma_4 = 2\lambda_1\left(\mathfrak{Re}(\lambda_4)|\lambda_2|^2 + \mathfrak{Re}(\lambda_2)|\lambda_4|^2\right) + |\lambda_2|^2|\lambda_4|^2 \ , \tag{2.20}$$

$$\Sigma_5 = \lambda_1|\lambda_2|^2|\lambda_4|^2 \ . \tag{2.21}$$

If all the real parts of the eigenvalues of $\mathcal{R}_{thermo}$ are strictly positive, one can easily check from the previous notations that:

$$\forall\, n \in [\![1,5]\!], \quad \Sigma_n > 0 \tag{2.22}$$

Case 3. Three eigenvalues of $\mathcal{R}_{thermo}$ are real: λ_1, λ_2 and λ_3. The remaining two are complex conjugate $\lambda_5 = \overline{\lambda_4}$. Thus, coefficients $\Sigma_n,\ n \in [\![1,5]\!]$ write:

$$\Sigma_1 = \lambda_1 + \lambda_2 + \lambda_3 + 2\mathfrak{Re}(\lambda_4) \ , \tag{2.23}$$

$$\Sigma_2 = (\lambda_1\lambda_2 + \lambda_1\lambda_3 + \lambda_2\lambda_3) + 2\left(\lambda_1 + \lambda_2 + \lambda_3\right)\mathfrak{Re}(\lambda_4) + |\lambda_4|^2 \ , \tag{2.24}$$

$$\Sigma_3 = \lambda_1\lambda_2\lambda_3 + 2\left(\lambda_1\lambda_2 + \lambda_1\lambda_3 + \lambda_2\lambda_3\right)\mathfrak{Re}(\lambda_4) + \left(\lambda_1 + \lambda_2 + \lambda_3\right)|\lambda_4|^2 \ , \tag{2.25}$$

$$\Sigma_4 = 2\lambda_1\lambda_2\lambda_3\mathfrak{Re}(\lambda_4) + \left(\lambda_1\lambda_2 + \lambda_1\lambda_3 + \lambda_2\lambda_3\right)|\lambda_4|^2 \ , \tag{2.26}$$

$$\Sigma_5 = \lambda_1\lambda_2\lambda_3|\lambda_4|^2 \ . \tag{2.27}$$

If all the real parts of the eigenvalues of $\mathcal{R}_{thermo}$ are strictly positive, we can once again easily check from the previous notations that:

$$\forall\, n \in [\![1,5]\!], \quad \Sigma_n > 0 \tag{2.28}$$

■

Remark 2.1.

(i) Necessary conditions of effective relaxation (2.12), (2.13), (2.14), (2.15), (2.16) cannot be proved to always stand true for any EoS. They have therefore to be numerically tested. The counterpart of Property 2 has been exhibited in the framework of an immiscible two-phase flow model in [35]. In the latter reference, a detailed analysis of relaxation conditions is added when restricting to stiffened gases EoS for each phase.

(ii) The inner relaxation process has also been studied in [36], considering the hybrid two-phase flow model [38].

3. **Numerical scheme**

This parts aims at building a numerical strategy for computing approximate solutions of system (1.4). The overall strategy is close to the one detailed in [9]. However, the scheme proposed in the sequel differs in its treatment of the source terms.

First, let's recall the global numerical approach presented in [9] for the current model, but also used in [17, 33], among others, for a two-phase flow framework. This strategy consists in two steps:

- Compute an approximate solution of the following subsystem associated with the convective part of the model:

$$\begin{cases} \dfrac{\partial \alpha_k}{\partial t} + \mathcal{V}_I(W)\cdot\nabla\alpha_k = 0 \ , \\ \dfrac{\partial m_k}{\partial t} + \nabla\cdot(m_k U_k) = 0 \ , \\ \dfrac{\partial m_k U_k}{\partial t} + \nabla\cdot(m_k U_k\otimes U_k + \alpha_k P_k \mathcal{I}) + \displaystyle\sum_{l=1,l\neq k}^{3} \Pi_{kl}(W)\nabla\alpha_l = 0 \ , \\ \dfrac{\partial \alpha_k E_k}{\partial t} + \nabla\cdot(\alpha_k E_k U_k + \alpha_k P_k U_k) - \displaystyle\sum_{l=1,l\neq k}^{3} \Pi_{kl}(W)\dfrac{\partial \alpha_l}{\partial t} = 0 \ , \end{cases} \tag{3.1}$$

  using an *explicit* Riemman solver adapted for non-conservative products. This first step fully determines the time step Δt. Details of this step can be found in [9].

- Then, solve with a *linear-implicit* scheme (on a time step Δt) the stiff system (2.2). It is the counterpart of (1.4) without the convective terms. In [9], this step is conducted with a fractional step approach, which decouples all relaxation effects for velocity, pressure, temperature, Gibbs free energy. The new approach proposed here follows the same strategy as the one in [35] in the framework of an immiscible two-phase flow model [3].

To begin with, as in [35], we take advantage of the block triangular structure of $\mathcal{R}^{relax}$. Indeed, as the velocity relaxation is less coupled with the other relaxation effects, we choose to treat it beforehand with the same method as the one presented in [9] and recalled in Appendix C.

In the sequel, in order to ease notations, the instant right after the velocity relaxation will be referred as t^n.

Then, (2.2) becomes:

$$\begin{cases} \dfrac{\partial \alpha_k}{\partial t} = \displaystyle\sum_{l=1,l\neq k}^{3} K_{kl}(W)\Delta P_{kl} \ , \\ \dfrac{\partial m_k}{\partial t} = -\displaystyle\sum_{l=1,l\neq k}^{3} \Lambda_{kl}(W)\Delta g_{kl} \ , \\ \dfrac{\partial m_k U_k}{\partial t} = -\displaystyle\sum_{l=1,l\neq k}^{3} V_{kl}\Lambda_{kl}(W)\Delta g_{kl} \ , \\ \dfrac{\partial \alpha_k E_k}{\partial t} - \displaystyle\sum_{l=1,l\neq k}^{3} \Pi_{kl}(W)\dfrac{\partial \alpha_l}{\partial t} = -\displaystyle\sum_{l=1,l\neq k}^{3} q_{kl}(W)\Delta T_{kl} \ - \displaystyle\sum_{l=1,l\neq k}^{3} H_{kl}\Lambda_{kl}(W)\Delta g_{kl} \ . \end{cases} \tag{3.2}$$

We also have the conservation law of the sum of the total energies (2.9).

From system (3.2), one can obtain:

$$m_k \partial_t \left(\frac{U_k^2}{2} \right) = -U_k \sum_{l \neq k} (V_{kl} - U_k) \, \Lambda_{kl}(W) \Delta g_{kl} \ . \tag{3.3}$$

Thus, using (1.22), we have:

$$\partial_t \left(\frac{1}{2} m_k U_k^2 \right) = - \sum_{l \neq k} H_{kl} \Lambda_{kl}(W) \Delta g_{kl} \ . \tag{3.4}$$

Therefore, from (3.2), we get:

$$\partial_t \left(m_k \epsilon_k \right) - \sum_{l=1, l \neq k}^{3} \Pi_{kl}(W) \frac{\partial \alpha_l}{\partial t} = - \sum_{l=1, l \neq k}^{3} q_{kl}(W) \Delta T_{kl} \ . \tag{3.5}$$

Then, a conservation law for the sum of the internal energies ϵ_k weighted by the partial densities m_k can be deduced and reads:

$$\partial_t \left(\sum_{k=1}^{3} m_k \epsilon_k \right) = 0 \ . \tag{3.6}$$

We also recall that the immiscible constraint (1.1) always stands true and can be seen as a stationary constraint:

$$\partial_t \left(\alpha_1 + \alpha_2 + \alpha_3 \right) = 0 \ . \tag{3.7}$$

Next, as in the previous part, an evolution equation of the quantity:

$$\Delta_{thermo} = (\Delta P_{12}, \Delta P_{13}, \Delta T_{12}, \Delta T_{13}, \Delta g_{23})^\intercal \ , \tag{3.8}$$

is constructed from (3.2):

$$\partial_t \left(\Delta_{thermo} \right) = - \mathcal{R}_{thermo} \Delta_{thermo} \ , \tag{3.9}$$

where $\mathcal{R}_{thermo}$ is the sub-matrix of $\mathcal{R}^{relax} \in \ \mathcal{M}_5(\mathbb{R})$ arising in (2.5). We recall that coefficients of matrix $\mathcal{R}^{relax}$ are given in Appendix B. Alongside (3.9) and still considering (3.6), (2.6), (2.7) and (1.1), the following can also be obtained from (3.2):

$$\partial_t \left(m_1 U_1 \right) = 0 \tag{3.10}$$

$$\partial_t \left(m_2 U_2 + m_3 U_3 \right) = 0 \tag{3.11}$$

To summarize, we end up with eleven unknowns, six steady constraints (2.9), (3.6), (2.6), (2.7), (3.10), (3.11) and the set of ODEs (3.9) Eventually, the new algorithm writes as:

Algorithm: *(Coupled P-T-g algorithm)*

Step 1: Estimate the evolution of Δ_{thermo} through (3.9) by using an Euler implicit scheme with $\mathcal{R}_{thermo}$ frozen at time t^n:

$$\Delta_{thermo}^{n+1} = \left(\mathcal{I} + \Delta t \mathcal{R}_{thermo}^n \right)^{-1} \Delta_{thermo}^n . \tag{3.12}$$

Step 2: Setting: $\widetilde{M}_n = m_2^n + m_3^n$, compute the partial densities at time t^{n+1}:

$$\begin{cases} m_1^{n+1} = m_1^n \\ m_2^{n+1} = \dfrac{\widetilde{M}_n}{1 + \frac{(\tilde{M}_n - m_2^n)}{m_2^n} \exp\left(\frac{\Delta g_{23}^{n+1}}{\tau_{23}^m{}^n \Gamma_0} \Delta t \right)} > 0 \\ m_3^{n+1} = \widetilde{M}_n - m_2^{n+1} \end{cases} \tag{3.13}$$

Thus complying with the steady constraints (2.6), (2.7).

Step 3: Write:

$$P_2^{n+1} = P_1^{n+1} - \Delta P_{12}^{n+1} \ , \tag{3.14}$$
$$P_3^{n+1} = P_1^{n+1} - \Delta P_{13}^{n+1} \ , \tag{3.15}$$
$$T_2^{n+1} = T_1^{n+1} - \Delta T_{12}^{n+1} \ , \tag{3.16}$$
$$T_3^{n+1} = T_1^{n+1} - \Delta T_{13}^{n+1} \ , \tag{3.17}$$
$$\tag{3.18}$$

and note, with help of (3.6):

$$\xi_n := \sum_{k=1}^{3} (m_k \epsilon_k)^n = \sum_{k=1}^{3} (m_k \epsilon_k)^{n+1}. \tag{3.19}$$

Then, find P_1^{n+1} and T_1^{n+1} in the admissible range, solutions of the implicit *non-linear* system composed of the discrete counterpart of (3.6):

$$m_1^{n+1}\epsilon_1(P_1^{n+1}, T_1^{n+1}) + m_2^{n+1}\epsilon_2(P_2^{n+1}, T_2^{n+1}) + m_3^{n+1}\epsilon_3(P_3^{n+1}, T_3^{n+1}) = \xi_n \ , \tag{3.20}$$

and the discrete counterpart of (1.1):

$$\frac{m_1^{n+1}}{\rho_1(P_1^{n+1}, T_1^{n+1})} + \frac{m_2^{n+1}}{\rho_2(P_2^{n+1}, T_2^{n+1})} + \frac{m_3^{n+1}}{\rho_3(P_3^{n+1}, T_3^{n+1})} = 1 \ . \tag{3.21}$$

Step 4: Update local variables P_2^{n+1}, P_3^{n+1}, T_2^{n+1}, T_3^{n+1}, α_1^{n+1}, α_2^{n+1}, α_3^{n+1}:

$$P_2^{n+1} = P_1^{n+1} - \Delta P_{12}^{n+1} \ , \tag{3.22}$$
$$P_3^{n+1} = P_1^{n+1} - \Delta P_{13}^{n+1} \ , \tag{3.23}$$
$$T_2^{n+1} = T_1^{n+1} - \Delta T_{12}^{n+1} \ , \tag{3.24}$$
$$T_3^{n+1} = T_1^{n+1} - \Delta T_{13}^{n+1} \ , \tag{3.25}$$
$$\alpha_1^{n+1} = \frac{m_1^{n+1}}{\rho_1(P_1^{n+1}, T_1^{n+1})} \ , \tag{3.26}$$
$$\alpha_2^{n+1} = \frac{m_2^{n+1}}{\rho_2(P_2^{n+1}, T_2^{n+1})} \ , \tag{3.27}$$
$$\alpha_3^{n+1} = 1 - \alpha_1^{n+1} - \alpha_2^{n+1} = \frac{m_3^{n+1}}{\rho_3(P_3^{n+1}, T_3^{n+1})} \ . \tag{3.28}$$

Step 5: Then, setting: $\Gamma_{23} = \Lambda_{23}\Delta g_{23}$, compute U_2^{n+1} and U_3^{n+1} as solutions of:

$$\begin{cases} (m_2U_2)^{n+1} - (m_2U_2)^n = \Delta t \dfrac{\Gamma_{23}^{n+1}}{2}(U_2^{n+1} + U_3^{n+1}) \ , \\ (m_3U_3)^{n+1} - (m_3U_3)^n = -\Delta t \dfrac{\Gamma_{23}^{n+1}}{2}(U_2^{n+1} + U_3^{n+1}) \ , \end{cases} \tag{3.29}$$

Step 6: Update the total energies as (using conservation law (2.9)):

$$\begin{cases} (\alpha_2E_2)^{n+1} = m_2^{n+1}\epsilon_2(P_2^{n+1}, T_2^{n+1}) + \dfrac{1}{2}m_2^{n+1}(U_2^{n+1})^2 \ , \\ (\alpha_3E_3)^{n+1} = m_3^{n+1}\epsilon_3(P_3^{n+1}, T_3^{n+1}) + \dfrac{1}{2}m_3^{n+1}(U_3^{n+1})^2 \ , \\ (\alpha_1E_1)^{n+1} = (\alpha_1E_1)^n + (\alpha_2E_2)^n + (\alpha_3E_3)^n - (\alpha_2E_2)^{n+1} - (\alpha_3E_3)^{n+1} \ . \end{cases} \tag{3.30}$$

Property 3 (The Coupled P-T-g algorithm)**.**

- *If the discrete relaxation process is effective over time, then the principal minors* Σ_i *,* $i \in [\![1,5]\!]$ *of matrix* $\mathcal{R}_{thermo}$ *are positive at each instant and at every point.*
- *For a mixture of three perfect gases (EoS), solutions of* (3.20) *and* (3.21) *exist and are unique inside their definition domain. Moreover,* (3.21) *ensures that, for* $k \in [\![1,3]\!]$*,* α_k *stays in* $]0,1[$*.*

The proof is similar to the one given in [35]. We briefly recall the main guidelines:

Proof.

- The first item is the discrete counterpart of Property 2. Indeed, if the thermodynamic relaxation is effective at time t^n, then the real parts of the eigenvalues of $\mathcal{R}^n_{thermo}$ are positive and therefore, (3.12) ensures a contraction of Δ_{thermo}.
- Consider a mixture of three perfect gases, $k \in \{1,3\}$:
$$P_k = \rho_k(\gamma_k - 1)\epsilon_k \ , \tag{3.31}$$
$$C_{v_k} T_k = \epsilon_k \ . \tag{3.32}$$
Thus equation (3.20) degenerates into:
$$m_1^{n+1} C_{v_1} T_1^{n+1} + m_2^{n+1} C_{v_2}(T_1^{n+1} - \Delta T_{12}^{n+1}) + m_3^{n+1} C_{v_2}(T_1^{n+1} - \Delta T_{13}^{n+1}) = \xi_n \ , \tag{3.33}$$
which can be solved directly and gives a positive T_1^{n+1}.
Then, a classical function analysis of (3.21) shows that there exists a unique solution of P_1^{n+1} which lays inside its definition domain. ∎

Remark 3.1. The first item of Property 3 can be seen as a way to numerically check if the relaxation process is effective or not in a test case at any time and everywhere. Indeed, coefficients Σ_i, for $i \in [\![1,5]\!]$ correspond to the coefficients of the characteristic polynomial of $\mathcal{R}_{thermo}$:
$$P_5(\lambda) = \lambda^5 - \Sigma_1\lambda^4 + \Sigma_2\lambda^3 - \Sigma_3\lambda^2 + \Sigma_4\lambda - \Sigma_5 \ , \tag{3.34}$$
and thus can be identified to the principal minors of $\mathcal{R}_{thermo}$. Those quantities Σ_i $i \in [\![1,5]\!]$ can be calculated directly from $\mathcal{R}_{thermo}$. In practice, we use *Maxima* [45], a computer algebra system to compute Σ_i , $i \in [\![1,5]\!]$.

4. Numerical Results

This part can be broken down into two main subsections. The first one aims at testing only the new algorithm presented above for treating the thermodynamic part of the source terms. The second part seeks to evaluate the new algorithm (coupled with the velocity relaxation algorithm described in Appendix C and the convective solver from [9]) against an experimental test case of a vapour explosion referred as KROTOS 44 [39]. Numerical results of this test case will also be compared to [9], where a similar numerical simulation is conducted.

4.1. The homogeneous case

In this subsection, we consider a flow, such that:
$$\forall\ k \in [\![1,3]\!], \quad U_k = 0 \ , \tag{4.1}$$
$$\forall\ k \in [\![1,3]\!],\ \forall\ \Psi_k \in \{\alpha_k, P_k, T_k, \alpha_k E_k\}, \quad \nabla\Psi = 0. \tag{4.2}$$

It corresponds to a zero-dimensional flow where only the thermodynamic relaxation process takes place.

Then we choose:

$$\begin{cases} \mathcal{P}_0 = \alpha_1^0\alpha_2^0\left(\dfrac{\rho_1^0(c_1^0)^2}{\alpha_1^0}+\dfrac{\rho_2^0(c_2^0)^2}{\alpha_2^0}\right)+\alpha_1^0\alpha_3^0\left(\dfrac{\rho_1^0(c_1^0)^2}{\alpha_1^0}+\dfrac{\rho_3^0(c_3^0)^2}{\alpha_3^0}\right)+\alpha_2^0\alpha_3^0\left(\dfrac{\rho_2^0(c_2^0)^2}{\alpha_2^0}+\dfrac{\rho_3^0(c_3^0)^2}{\alpha_3^0}\right) \\ \Gamma_0 = \left| m_3^0\left(\gamma_2 C_{v_2}+\dfrac{\epsilon_{2_0}}{T_2^0}\left(2+\dfrac{\epsilon_{2_0}}{C_{v_2}T_2^0}\right)\right)+m_2^0\left(\gamma_3 C_{v_3}+\dfrac{\epsilon_{3_0}}{T_3^0}\left(2+\dfrac{\epsilon_{3_0}}{C_{v_3}T_3^0}\right)\right)\right| \end{cases} \tag{4.3}$$

All relaxation time scales are supposed to be constant in this sub-section. Moreover, they are taken to be equal on each phasic link:

$$\forall\ \Psi \in P,T: \quad \tau_{12}^{\Psi}=\tau_{13}^{\Psi}=\tau_{23}^{\Psi}=\tau^{\Psi}\ , \tag{4.4}$$

and

$$\tau_{23}^{m}=\tau^{m}. \tag{4.5}$$

The values of the relaxation time scales which will be used in the numerical simulation are given in Appendix A.

For all numerical simulations we will use stiffened gas EoS within each phase:

$$P_k+\gamma_k\Pi_k=\rho_k(\gamma_k-1)(\epsilon_k-\epsilon_{0,k})\ , \tag{4.6}$$

The EoS coefficients are also given in Appendix A.

Eventually, we refer the reader to Appendix A regarding the initial conditions of the numerical test cases. Two test cases are computed. The only difference between case A and case B is the value of the pressure relaxation time scale.

Figures 4.1, 4.2, 4.3 and 4.4 show that the effective relaxation time scale of the global system is significantly larger than the biggest relaxation time scale among τ^P, τ^T, τ^m, which is 10^{-2}s here. A similar behaviour has already been pointed out for a two-phase flow model in [35] and a detailed analysis is proposed in Appendix A of [41] for a two-phase flow model without mass transfer. Moreover, even for a coarse time step, the method captures rather well the behaviour of the solution for both cases. Figures 4.1 and 4.3 show the impact of the choice of the pressure relaxation time scale on the behaviour of the solution. Indeed, in case A, the pressure relaxation time scale is 1000 times larger than the one used in case B, therefore, bigger discrepancies between phasic pressure profiles in case A than in case B are expected. However the magnitude of this change cannot be *a priori* estimated. Up to the authors, it advocates to avoid making strong assumptions on the relaxation time scales, when aiming at a fair representation of the transient regime.

We emphasize that the fractional step algorithm presented in [9] is not stable enough to compute solutions of test case A.

Eventually, a convergence test is presented in Figure 4.5. As no analytical solution of system (3.2) can be exhibited, the solution is compared to a refined computation, with a time step $dt_{cv}=10^{-10}s$ for a simulation of $10s$. The error of a quantity κ, $E_\kappa(dt, t=t_{transient})$ is thus defined as:

$$E_\kappa(dt,t=t_{transient})=\frac{|\kappa_{dt}(t=t_{transient})-\kappa_{dt_{cv}}(t=t_{transient})|}{\kappa_{dt_{cv}}(t=t_{transient})}, \tag{4.7}$$

with $\kappa_{dt}(t=t_{transient})$ the value of κ at time $t=t_{transient}$ computed with the numerical scheme presented in Section 3 using a time step dt. Figure 4.5 shows that a convergence rate close to 1 is retrieved.

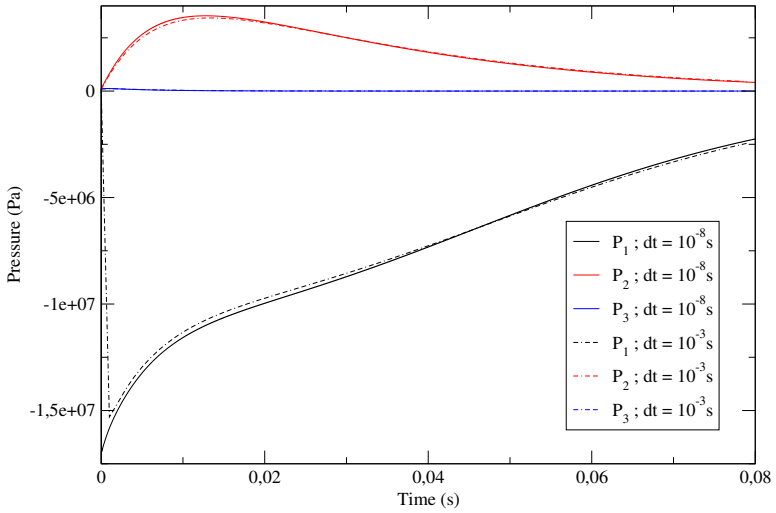

FIGURE 4.1. Pressure evolution for case A ($\tau^P = 10^{-5}s$, $\tau^T = 10^{-3}s$ and $\tau^m = 10^{-2}s$) computed with two different time step sizes: $\Delta t = 10^{-8}s$ and $\Delta t = 10^{-3}s$ (dashed lines).

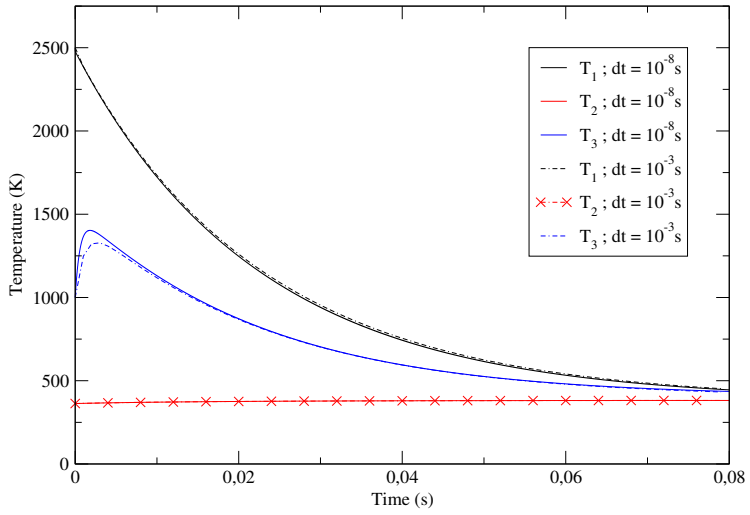

FIGURE 4.2. Temperature evolution for case A ($\tau^P = 10^{-5}s$, $\tau^T = 10^{-3}s$ and $\tau^m = 10^{-2}s$) computed with two different time step sizes: $\Delta t = 10^{-8}s$ and $\Delta t = 10^{-3}s$ (dashed lines).

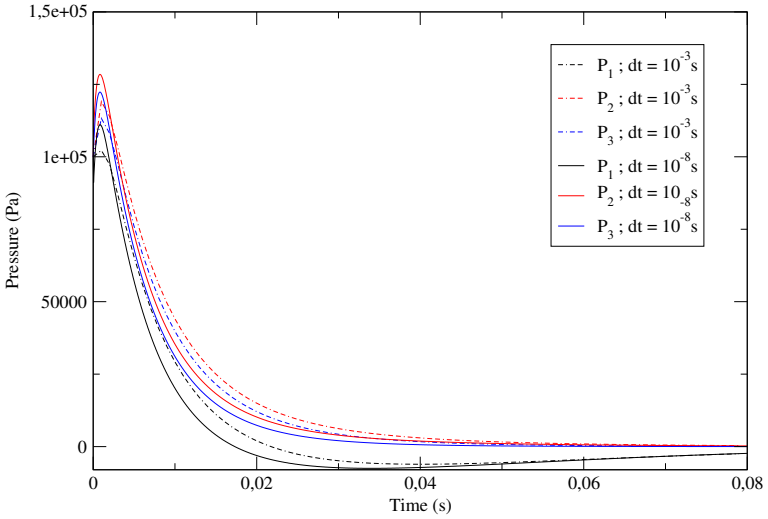

FIGURE 4.3. Pressure evolution for case B ($\tau^P = 10^{-8}s$, $\tau^T = 10^{-3}s$ and $\tau^m = 10^{-2}s$) computed with two different time step sizes: $\Delta t = 10^{-8}s$ and $\Delta t = 10^{-3}s$ (dashed lines).

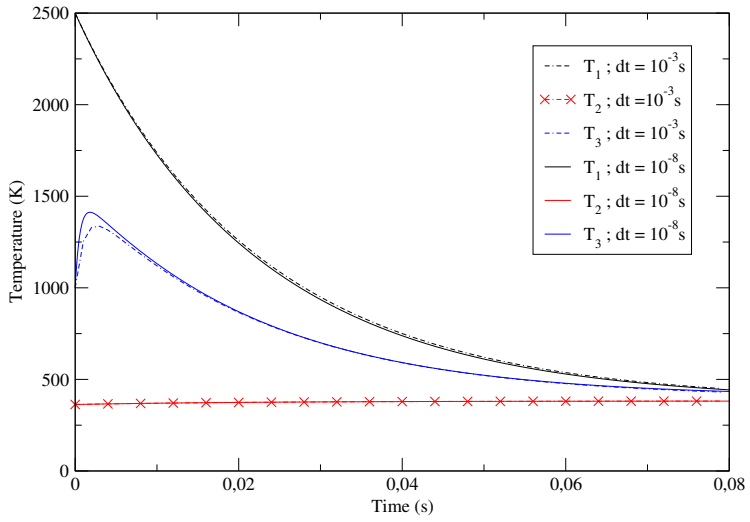

FIGURE 4.4. Temperature evolution for case B ($\tau^P = 10^{-8}s$, $\tau^T = 10^{-3}s$ and $\tau^m = 10^{-2}s$) computed with two different time step sizes: $\Delta t = 10^{-8}s$ and $\Delta t = 10^{-3}s$ (dashed lines).

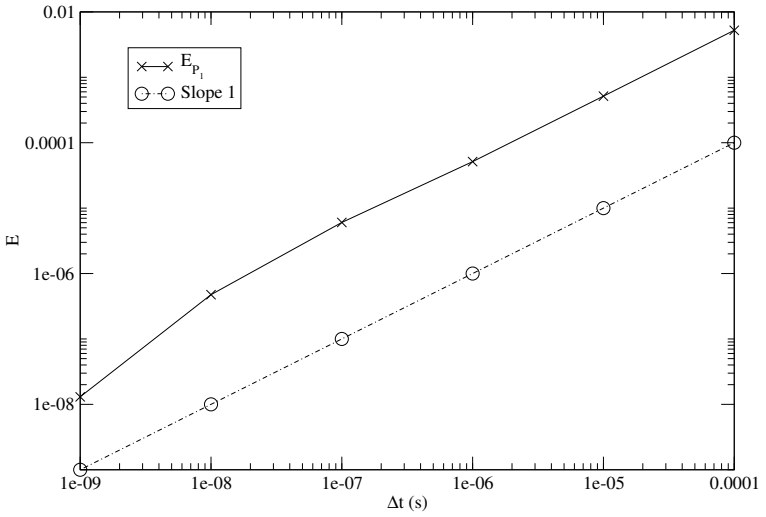

FIGURE 4.5. Convergence curve on the pressure P_1 in case A.

4.2. **Application to KROTOS 44 set up** [39]

This Section aims at simulating a KROTOS 44 type set up. The set up consists in a one dimension shock tube in water where droplets of liquid corium (phase 1) interact with liquid water (phase 2) and water vapour (phase 3), as shown in Figure 4.6.

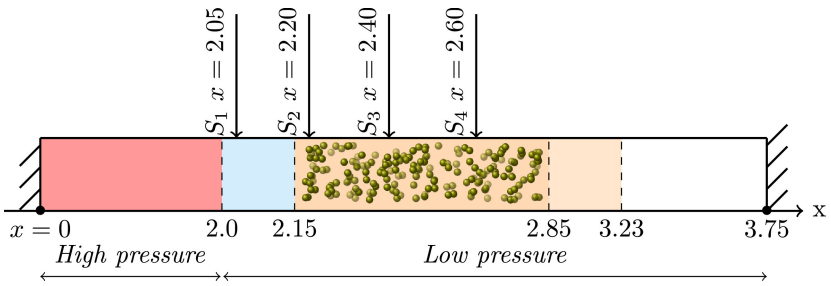

FIGURE 4.6. Scheme of the KROTOS-like shock tube

First, at time $t = 0$, velocities are supposed to be null:

$$\forall\, x \in [0.0, 3.75],\ \forall\, k \in [\![1, 3]\!], \quad U_k(x, t = 0) = 0 \tag{4.8}$$

Moreover, at time $t = 0$, pressures are initialized in the *high pressure* chamber, see Figure 4.6, as:

$$\forall\, x \in [0.0, 2.0],\ \forall\, k \in [\![1, 3]\!], \quad P_k(x, t = 0) = 150\,\text{bar} \tag{4.9}$$

whereas in the *low pressure* chamber, they are set as:

$$\forall\, x \in [2.0, 3.75],\ \forall\, k \in [\![1, 3]\!], \quad P_k(x, t = 0) = 1\,\text{bar} \tag{4.10}$$

Introducing $\epsilon_{lim} = 10^{-6}$, the initial conditions are given in Table 4.1:

Table 4.1. Initial conditions of the numerical experiment

Abscissa interval (m)	α_1	α_2	α_3	T_1 (K)	T_2 (K)	T_3 (K)
High pressure: $x \in [0.0, 2.0]$	ϵ_{lim}	$1 - 2\epsilon_{lim}$	ϵ_{lim}	1000	1000	1000
Pure liquid: $x \in]2.0, 2.15]$	ϵ_{lim}	$1 - 2\epsilon_{lim}$	ϵ_{lim}	363	363	363
Interaction: $x \in]2.15, 2.85]$	0.026	0.884	0.09	2500	363	1000
Plug: $x \in]2.85, 3.23]$	ϵ_{lim}	0.835 - ϵ_{lim}	0.165	363	363	363
Cover gas: $x \in]3.23, 3.75]$	ϵ_{lim}	ϵ_{lim}	$1 - 2\epsilon_{lim}$	363	363	700

Besides, four numerical probes are set up:

- S_1 is placed at the beginning of the *pure liquid* zone: $x = 2.05\,\text{m}$,
- S_2 is located at the beginning of the *interaction* zone: $x = 2.20\,\text{m}$,
- S_3 is situated at one third of the *interaction* zone: $x = 2.40\,\text{m}$,
- S_4 is positioned at two third of the *interaction* zone: $x = 2.60\,\text{m}$.

Before going further on, as in [35], we need to introduce an evolution equation of the interfacial area $\mathcal{A}_1$ for liquid corium droplets:

$$\mathcal{A}_1 = \frac{6\alpha_1}{D_1} \tag{4.11}$$

where D_1 stands for the diameter of the corium droplets, which is initialized along the tube at time $t = 0$ as: $D_1 = 15\,\text{mm}$. Indeed, as shown physically in [25] and numerically in [9, 13, 35], taking into account droplet atomization is crucial in order to predict well the energy transfer between phases and therefore to have numerical solutions close to the experimental data. The equation of evolution of the interfacial area (see Appendix D) and its numerical treatment are taken from [8].

We now need to specify for $(k, l) \in [\![1, 3]\!]\ , l > k$ the form of the relaxation time scales τ_{kl}^U, τ_{kl}^P, τ_{kl}^T and τ_{kl}^m. On each phasic connection, their form is:

- Velocity relaxation time scales:

$$\frac{1}{\tau_{12}^U} = \frac{1}{\tau_{21}^U} = \frac{0.75 C_{d_{12}}(m_1 + m_2)\|U_1 - U_2\|}{\rho_1 D_1}\ ; \tag{4.12}$$

$$\frac{1}{\tau_{13}^U} = \frac{1}{\tau_{31}^U} = \frac{0.75 C_{d_{13}}(m_1 + m_3)\|U_1 - U_3\|}{\rho_1 D_1}\ ; \tag{4.13}$$

$$\frac{1}{\tau_{23}^U} = \frac{1}{\tau_{32}^U} = \frac{0.75 C_{d_{23}}(m_2 + m_3)\|U_2 - U_3\|}{\rho_3 D_3}\ . \tag{4.14}$$

This expression of τ_{kl}^U is derived from the Stokes formula [40]. $C_{d_{kl}} = 24/Re_{kl}$ is the drag coefficient. The Reynolds number Re_{kl} is defined as:

$$Re_{12} = \frac{\rho_2 D_1 \|U_1 - U_2\|}{\mu_2} \tag{4.15}$$

$$Re_{13} = \frac{\rho_3 D_1 \|U_1 - U_3\|}{\mu_3} \tag{4.16}$$

$$Re_{23} = \frac{\rho_2 D_3 \|U_2 - U_3\|}{\mu_2} \tag{4.17}$$

D_1 and D_3 are the diameter of the corium droplets and the vapour droplets respectively. The diameter of the corium droplet is obtained through an interfacial area equation whereas the liquid vapour one is supposed constant: $D_3 = 15\,\text{mm}$.

- Pressure relaxation time scales:

$$\frac{1}{\mathcal{P}_0\tau_{12}^P} = \frac{1}{\mathcal{P}_0\tau_{21}^P} = \frac{3}{4\pi\mu_2}\ ; \tag{4.18}$$

$$\frac{1}{\mathcal{P}_0\tau_{13}^P} = \frac{1}{\mathcal{P}_0\tau_{31}^P} = \frac{3}{4\pi\mu_3}\ ; \tag{4.19}$$

$$\frac{1}{\mathcal{P}_0\tau_{23}^P} = \frac{1}{\mathcal{P}_0\tau_{32}^P} = \frac{3}{4\pi\mu_2}\ . \tag{4.20}$$

where $\mu_2 = 2.82\ \cdot 10^{-4}\,\text{kg}\,\text{m}^{-1}\text{s}^{-1}$ and $\mu_3 = 1.8\ \cdot 10^{-5}\,\text{kg}\,\text{m}^{-1}\text{s}^{-1}$ are the dynamic viscosity of respectively the liquid water and liquid vapour at 1 bar and 293 K. It is the limit of the closure law proposed in [23] for small diameter droplets.

- Temperature relaxation time scales:

$$\frac{1}{\tau_{12}^T} = \frac{1}{\tau_{21}^T} = \frac{6\alpha_1 Nu_1\lambda_1(m_1C_{v_1} + m_2C_{v_2})}{m_1C_{v_1}m_2C_{v_2}D_1^2}\ ; \tag{4.21}$$

$$\frac{1}{\tau_{13}^T} = \frac{1}{\tau_{31}^T} = \frac{6\alpha_1 Nu_1\lambda_1(m_1C_{v_1} + m_3C_{v_3})}{m_1C_{v_1}m_3C_{v_3}D_1^2}\ ; \tag{4.22}$$

$$\frac{1}{\tau_{23}^T} = \frac{1}{\tau_{32}^T} = \frac{6\alpha_3 Nu_3\lambda_3(m_2C_{v_2} + m_3C_{v_3})}{m_2C_{v_2}m_3C_{v_3}D_3^2}\ . \tag{4.23}$$

where $Nu_1 = 10$, $Nu_3 = 10$ are the Nusselt number of the corium and the water vapour respectively and $\lambda_1 = 230\ (\text{W}\,\text{m}^{-1}\text{K}^{-1})$ and $\lambda_2 = 0.6\ (\text{W}\,\text{m}^{-1}\text{K}^{-1})$ are the thermal conductivity of the corium and liquid vapour respectively. This form is taken from [46, 51, 52, 60].

- Gibbs potential relaxation time scale τ_{23}^m is supposed to be constant:

$$\tau_{23}^m = \tau^m = 10^{-5}s\ . \tag{4.24}$$

Defining $T_k^{I,0} = T_k(x \in]2.15, 2.85], t = 0)$, coefficient Γ_0 is here taken as follows:

$$\Gamma_0 = \left| m_3^0\left(\gamma_2 C_{v_2} + \frac{\epsilon_{2_0}}{T_2^{I,0}}\left(2 + \frac{\epsilon_{2_0}}{C_{v_2}T_2^{I,0}}\right)\right) + m_2^0\left(\gamma_3 C_{v_3} + \frac{\epsilon_{3_0}}{T_3^{I,0}}\left(2 + \frac{\epsilon_{3_0}}{C_{v_3}T_3^{I,0}}\right)\right)\right|. \tag{4.25}$$

As we can see on Figures 4.7 and 4.8, the total pressure $P_{mix} = \sum_{k=1}^{3}\alpha_k P_k$ peaks at station 3 at 60.9 MPa, which is close to the measured total pressure interval in [39] (50 MPa to 60 MPa). A similar test case has been computed in [9] but as the relaxation is supposed to be instantaneous for both pressure and velocity, the pressure peak was far lower than the one computed here. We note that, oscillations come up at the beginning of the simulation, especially at station 3. Those oscillations occur as eigenvalues of the relaxation matrix $\mathcal{R}_{thermo}$ become complex conjugate. The coarse mesh can hardly capture the structure after the shock. The difference on the total pressure plateau between the two refined meshes (respectively 10 000 cells and 20 000 cells) is about 2% for station 3 and 1% for station 2.

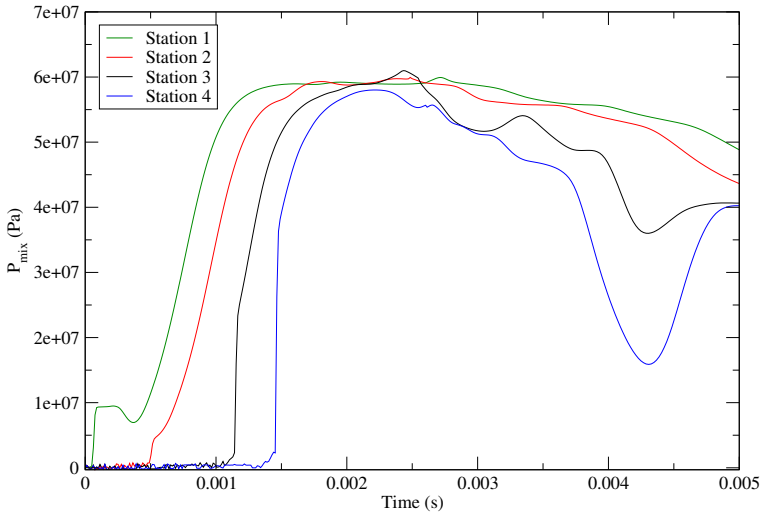

FIGURE 4.7. Evolution of the pressure P_{mix} at the four stations of the Krotos like experiment for a mesh including 20 000 cells.

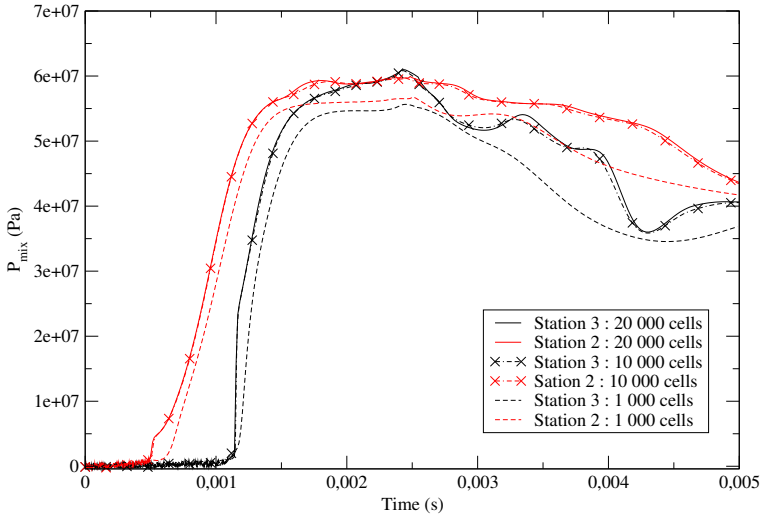

FIGURE 4.8. Evolution of the total pressure on station 2 (red lines) and 3 (black lines) for three meshes including respectively 1000 cells, 10 000 cells and 20 000 cells.

Eventually, as shown in Figure 4.9, the droplet break-up is active throughout the simulation.

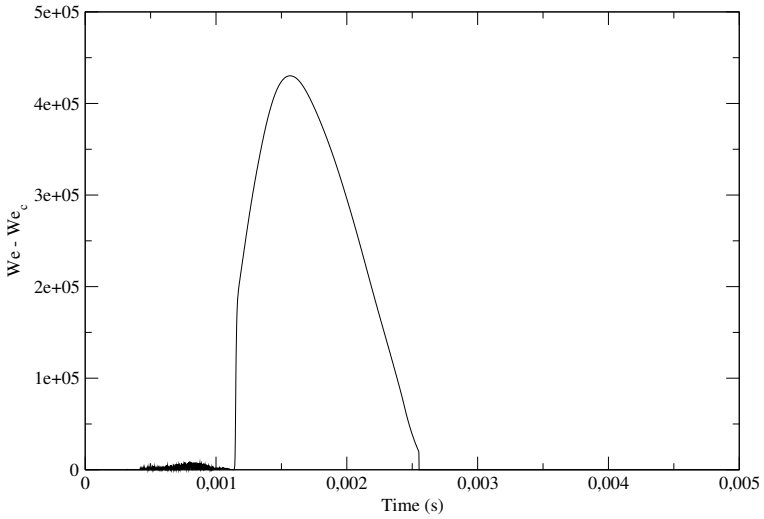

FIGURE 4.9. Evolution of the difference $We - We_c$ at station 3 with a mesh including 10 000 cells

5. **Conclusion**

When tackling vapour explosion applications, we may conclude that the algorithms presented in this article, in order to account for source terms, enable us to obtain convergent approximations of solutions of the three-phase flow model [30, 47], when the mesh is refined. We recall here that the former algorithms detailed in reference [9] lead to a failure of the computer code, in a similar framework.

We would like to recall that the emphasis of this work is on providing *stable* numerical schemes for tackling steam explosion. Thus, for future work, investigating some more sophisticated ODE integrators could increase the accuracy of the numerical scheme. For example, a Radau 5 method (see [59]) could be used for solving system (36). Other implicit high-order methods for solving ODE could also be investigated (see [12]).

Obviously, the temptation is now great to extend the relaxation schemes developed in [16] for the convective effect of the two-phase flow model [3] (respectively for a barotropic three-phase flow in [55]), to the immiscible three-phase flow models with energy [30]. The reader is referred to [16] for a comparison of the capabilities of schemes introduced in [56] and [58], when focusing on the two-phase flow model [3].

Moreover, more complex/realistic EoS might be considered in the second step on the algorithm, instead of the simple SGG EoS considered herein. In that case, it would however remain to prove that existence and uniqueness of the discrete solution of Step 2 (in the admissible state space) would hold true.

Eventually, the authors emphasize again that in this work, no strong assumption on the relaxation time scales underlies the model (such as in [20, 21, 44] for the two-phase flow framework), or the treatment of the source terms (as in [27, 48, 49] for the two-phase flow framework). However, beyond this, it urges the question of the accurate modeling of those relaxation time scales, and more generally the question of the modeling of the source terms. Actually, few closure laws for the two-phase flow framework exist in the literature, see for example [6, 10, 23, 40, 54]. Furthermore, we know that those time scales play a key role on the transient of the flow, see Figures 4.1, 4.3 and Appendix A of [41].

Therefore, even in the two-phase flow framework, a parametric study scanning the whole range of the four relaxation time scales is a work that remains to be done, using very fine meshes, for a better understanding of the impact of these time scales on the stability of solutions of these ODEs and beyond of PDEs. This seems to be a important work in order to better understand the multiphase flow models.

Moreover, other source terms than the ones used in this paper have been proposed in the literature, and an attempt to compare some of them in the two-phase flow framework has been conducted in [11]. An extension of this study to the three-phase flow framework still remains to be achieved.

Acknowledgments

This work has been achieved during the PhD thesis of the second author at EDF Lab Chatou and Aix-Marseille University, with partial financial support from ANRT under EDF-CIFRE contract number 2020-0946. Computational facilities were provided by EDF. The second author would also like to thank the CEA, and especially Maria-Giovanna Rodio, for giving him the time to finish writing the article.

Appendix A. Numerical parameters

Table A.1. EoS coefficients for all of the conducted simulations

	Phase 1	Phase 2	Phase 3
C_v	1.2872948262582229e+01	1.452904592629688e+03	4.441148752333071e+03
γ	2.2838590974110350e+01	1.614924811807376e+00	1.085507894797296e+00
$\widehat{\Pi}$	1.8847923625716622e+09	3.563521398523755e+08	0.0
ϵ_0	−1.3316200000000000e+05	0.0	0.0
s_0	0.0	0.0	−4.769786773517021e+04

Table A.2. Initial conditions for the homogeneous cases

$P_1(t=0)$	1.0 bar
$P_2(t=0)$	1.0 bar
$P_3(t=0)$	1.0 bar
$T_1(t=0)$	2500.0 K
$T_2(t=0)$	363.0 K
$T_3(t=0)$	1000.0 K
$\alpha_1(t=0)$	0.026
$\alpha_2(t=0)$	0.884
$\alpha_3(t=0)$	0.09

Table A.3. Numerical parameters for Case A and Case B in the homogeneous case.

	Case A	Case B
τ^P	1.0e-5 s	1.0e-8 s
τ^T	1.0e-3 s	1.0e-3 s
τ^m	1.0e-2 s	1.0e-2 s

Appendix B. Coefficients of the relaxation matrix

First, we define $\mathcal{R}^{relax}$ as:

$$\mathcal{R}^{relax}(W) = \begin{pmatrix} R_{UU}(W) & 0 & 0 & 0 \\ R_{PU}(W) & R_{PP}(W) & R_{PT}(W) & r_{Pg}(W) \\ R_{TU}(W) & R_{TP}(W) & R_{TT}(W) & r_{Tg}(W) \\ r_{gU}(W)^\intercal & r_{gP}(W)^\intercal & r_{gT}(W)^\intercal & r_g(W) \end{pmatrix}. \tag{B.1}$$

Matrices $R_{UU}(W)$, $R_{PU}(W)$, R_{PP}, $R_{PT}(W)$, $R_{TU}(W)$, $R_{TP}(W)$, $R_{TT}(W)$ are in $\mathcal{M}_2(\mathbb{R})$, whereas $r_{Pg}(W)$, $r_{Tg}(W)$, $r_{gU}(W)$, $r_{gP}(W)$, r_{gT} are in $\mathbb{R}^2$ and r_g is a scalar. Coefficients of $R_{UU}(W)(W)$ write as follows:

$$\begin{aligned} r_{UU_{11}} &= \frac{1}{m_1} d_{12} + \frac{1}{m_2}\left(d_{12} + d_{23} - \frac{\Lambda_{23}}{2}\Delta g_{23}\right) , \\ r_{UU_{12}} &= \frac{1}{m_1} d_{13} - \frac{1}{m_2}\left(d_{23} - \frac{\Lambda_{23}}{2}\Delta g_{23}\right) , \\ r_{UU_{21}} &= \frac{1}{m_1} d_{12} - \frac{1}{m_3}\left(d_{23} + \frac{\Lambda_{23}}{2}\Delta g_{23}\right) , \\ r_{UU_{22}} &= \frac{1}{m_1} d_{13} + \frac{1}{m_3}\left(d_{13} + d_{23} + \frac{\Lambda_{23}}{2}\Delta g_{23}\right) . \end{aligned} \tag{B.2}$$

Writing $\theta_k = m_k \left.\frac{\partial \epsilon_k}{\partial T_k}\right|_{\rho_k}$, and:

$$F_{21} = K_{12}\rho_1^2 \left.\frac{\partial \epsilon_1}{\partial \rho_1}\right|_{T_1} - P_2 K_{12} + (\Delta P_{12} - \Delta P_{13}) K_{23} , \tag{B.3}$$

$$F_{31} = K_{13}\rho_1^2 \left.\frac{\partial \epsilon_1}{\partial \rho_1}\right|_{T_1} - P_3 K_{13} - (\Delta P_{12} - \Delta P_{13}) K_{23} , \tag{B.4}$$

$$F_{22} = -(K_{12} + K_{23})\rho_2^2 \left.\frac{\partial \epsilon_2}{\partial \rho_2}\right|_{T_2} + P_2 (K_{23} + K_{12}) , \tag{B.5}$$

$$F_{32} = K_{23}\rho_2^2 \left.\frac{\partial \epsilon_2}{\partial \rho_2}\right|_{T_2} - P_2 K_{23} , \tag{B.6}$$

$$F_{23} = K_{23}\rho_3^2 \left.\frac{\partial \epsilon_3}{\partial \rho_3}\right|_{T_3} - P_3 K_{23} , \tag{B.7}$$

$$F_{33} = -(K_{13} + K_{23})\rho_3^2 \left.\frac{\partial \epsilon_3}{\partial \rho_3}\right|_{T_3} + P_3 (K_{23} + K_{13}) . \tag{B.8}$$

Moreover, setting $\sigma_k = m_k \left.\frac{\partial \epsilon_k}{\partial P_k}\right|_{\rho_k}$, and:

$$G_{21} = -K_{12}(\rho_1 c_1)^2 \left.\frac{\partial \epsilon_1}{\partial P_1}\right|_{\rho_1} + \Delta P_{12} K_{12} + (\Delta P_{12} - \Delta P_{13}) K_{23} \ , \tag{B.9}$$

$$G_{31} = -K_{13}(\rho_1 c_1)^2 \left.\frac{\partial \epsilon_1}{\partial P_1}\right|_{\rho_1} + \Delta P_{13} K_{13} - (\Delta P_{12} - \Delta P_{13}) K_{23} \ , \tag{B.10}$$

$$G_{22} = (K_{12} + K_{23})(\rho_2 c_2)^2 \left.\frac{\partial \epsilon_2}{\partial P_2}\right|_{\rho_2} \ , \tag{B.11}$$

$$G_{32} = -K_{23}(\rho_2 c_2)^2 \left.\frac{\partial \epsilon_2}{\partial P_2}\right|_{\rho_2} \ , \tag{B.12}$$

$$G_{23} = -K_{23}(\rho_3 c_3)^2 \left.\frac{\partial \epsilon_3}{\partial P_3}\right|_{\rho_3} \ , \tag{B.13}$$

$$G_{33} = (K_{13} + K_{23})(\rho_3 c_3)^2 \left.\frac{\partial \epsilon_3}{\partial P_3}\right|_{\rho_3} \ . \tag{B.14}$$

Coefficients of the sub-matrices of $\mathcal{R}^{relax}(W)$ read:

- $R_{TU}(W) =$

$$r_{TU_{11}} = \Delta U_{12} \left(\frac{d_{12} + d_{23}}{2\theta_2} - \frac{d_{12}}{2\theta_1} \right) - \frac{d_{23}}{2\theta_2} \Delta U_{13} \ , \tag{B.15}$$

$$r_{TU_{12}} = \Delta U_{13} \left(\frac{d_{23}}{2\theta_2} - \frac{d_{13}}{2\theta_1} \right) - \frac{d_{23}}{2\theta_2} \Delta U_{12} \ , \tag{B.16}$$

$$r_{TU_{21}} = \Delta U_{12} \left(\frac{d_{23}}{2\theta_3} - \frac{d_{12}}{2\theta_1} \right) - \frac{d_{23}}{2\theta_3} \Delta U_{13} \ , \tag{B.17}$$

$$r_{TU_{22}} = \Delta U_{13} \left(\frac{d_{13} + d_{23}}{2\theta_3} - \frac{d_{13}}{2\theta_1} \right) - \frac{d_{23}}{2\theta_3} \Delta U_{12} \ . \tag{B.18}$$

- $R_{TP}(W) =$

$$r_{TP_{11}} = -\frac{F_{21}}{\theta_1} + \frac{F_{22}}{\theta_2} \ , \tag{B.19}$$

$$r_{TP_{12}} = -\frac{F_{31}}{\theta_1} + \frac{F_{32}}{\theta_2} \ , \tag{B.20}$$

$$r_{TP_{21}} = -\frac{F_{21}}{\theta_1} + \frac{F_{23}}{\theta_3} \ , \tag{B.21}$$

$$r_{TP_{22}} = -\frac{F_{31}}{\theta_1} + \frac{F_{33}}{\theta_3} \ . \tag{B.22}$$

- $R_{TT}(W) =$

$$r_{TT_{11}} = \frac{q_{12}}{\theta_1} + \frac{q_{12} + q_{23}}{\theta_2} \ , \tag{B.23}$$

$$r_{TT_{12}} = \frac{q_{13}}{\theta_1} - \frac{q_{23}}{\theta_2} \ , \tag{B.24}$$

$$r_{TT_{21}} = -\frac{q_{23}}{\theta_3} + \frac{q_{12}}{\theta_1} \ , \tag{B.25}$$

$$r_{TT_{22}} = \frac{q_{13}}{\theta_1} + \frac{q_{13} + q_{23}}{\theta_3} \ . \tag{B.26}$$

- $r_{Tg}(W) =$

$$r_{Tg_1} = \frac{\Lambda_{23}}{\theta_2}\left(\epsilon_2 + \rho_2 \left.\frac{\partial \epsilon_2}{\partial \rho_2}\right|_{T_2}\right) , \tag{B.27}$$

$$r_{Tg_2} = -\frac{\Lambda_{23}}{\theta_3}\left(\epsilon_3 + \rho_3 \left.\frac{\partial \epsilon_3}{\partial \rho_3}\right|_{T_3}\right) . \tag{B.28}$$

- $R_{PU}(W) =$

$$r_{PU_{11}} = \Delta U_{12}\left(\frac{d_{12}+d_{23}}{2\sigma_2} - \frac{d_{12}}{2\sigma_1}\right) - \frac{d_{23}}{2\sigma_2}\Delta U_{13} , \tag{B.29}$$

$$r_{PU_{12}} = \Delta U_{13}\left(\frac{d_{23}}{2\sigma_2} - \frac{d_{13}}{2\sigma_1}\right) - \frac{d_{23}}{2\sigma_2}\Delta U_{12} , \tag{B.30}$$

$$r_{PU_{21}} = \Delta U_{12}\left(\frac{d_{23}}{2\sigma_3} - \frac{d_{12}}{2\sigma_1}\right) - \frac{d_{23}}{2\sigma_3}\Delta U_{13} , \tag{B.31}$$

$$r_{PU_{22}} = \Delta U_{13}\left(\frac{d_{13}+d_{23}}{2\sigma_3} - \frac{d_{13}}{2\sigma_1}\right) - \frac{d_{23}}{2\sigma_3}\Delta U_{12} . \tag{B.32}$$

- $R_{PP}(W) =$

$$r_{PP_{11}} = \frac{1}{m_1}\left((\rho_1 c_1)^2 K_{12} + \left(\left.\frac{\partial \epsilon_1}{\partial P_1}\right|_{\rho_1}\right)^{-1}(K_{23}\Delta P_{13} - (K_{12}+K_{23})\Delta P_{12})\right) + \frac{1}{m_2}(\rho_2 c_2)^2(K_{12}+K_{23}) , \tag{B.33}$$

$$r_{PP_{12}} = \frac{1}{m_1}\left(K_{13}(\rho_1 c_1)^2 + \left(\left.\frac{\partial \epsilon_1}{\partial P_1}\right|_{\rho_1}\right)^{-1}(K_{23}\Delta P_{12} - (K_{23}+K_{13})\Delta P_{13})\right) - \frac{1}{m_2}K_{23}(\rho_2 c_2)^2 , \tag{B.34}$$

$$r_{PP_{21}} = \frac{1}{m_1}\left((\rho_1 c_1)^2 K_{12} + \left(\left.\frac{\partial \epsilon_1}{\partial P_1}\right|_{\rho_1}\right)^{-1}(K_{23}\Delta P_{13} - (K_{12}+K_{23})\Delta P_{12})\right) - \frac{1}{m_3}K_{23}(\rho_3 c_3)^2 , \tag{B.35}$$

$$r_{PP_{22}} = \frac{1}{m_1}\left(K_{13}(\rho_1 c_1)^2 + \left(\left.\frac{\partial \epsilon_1}{\partial P_1}\right|_{\rho_1}\right)^{-1}(K_{23}\Delta P_{12} - (K_{23}+K_{13})\Delta P_{13})\right) + \frac{1}{m_3}(K_{13}+K_{23})(\rho_3 c_3)^2 . \tag{B.36}$$

- $R_{PT}(W) =$

$$r_{PT_{11}} = \frac{q_{12}}{\sigma_1} + \frac{q_{12}+q_{23}}{\sigma_2} , \tag{B.37}$$

$$r_{PT_{12}} = \frac{q_{13}}{\sigma_1} - \frac{q_{23}}{\sigma_2} , \tag{B.38}$$

$$r_{PT_{21}} = -\frac{q_{23}}{\sigma_3} + \frac{q_{12}}{\sigma_1} , \tag{B.39}$$

$$r_{PT_{22}} = \frac{q_{13}}{\sigma_1} + \frac{q_{13}+q_{23}}{\sigma_3} . \tag{B.40}$$

- $r_{Pg}(W) =$

$$r_{Pg_1} = \frac{\Lambda_{23}}{\sigma_2}\left(\epsilon_2 + \frac{P_2}{\rho_2} - \rho_2 c_2^2 \left.\frac{\partial \epsilon_2}{\partial P_2}\right|_{\rho_2}\right) , \tag{B.41}$$

$$r_{Pg_2} = -\frac{\Lambda_{23}}{\sigma_3}\left(\epsilon_3 + \frac{P_3}{\rho_3} - \rho_3 c_3^2 \left.\frac{\partial \epsilon_3}{\partial P_3}\right|_{\rho_3}\right) . \tag{B.42}$$

- $r_{gU}(W) =$

$$r_{gU_1} = -\frac{1}{2\rho_2 T_2}\left(\frac{1}{\sigma_2} - \frac{\rho_2 h_2}{\theta_2}\right)[d_{12}\Delta U_{12} + d_{23}(\Delta U_{12} - \Delta U_{13})] + \frac{d_{23}}{2\rho_3 T_3}\left(\frac{1}{\sigma_3} - \frac{\rho_3 h_3}{\theta_3}\right)[\Delta U_{12} - \Delta U_{13}] , \tag{B.43}$$

$$r_{gU_2} = -\frac{d_{23}}{2\rho_2 T_2}\left(\frac{1}{\sigma_2} - \frac{\rho_2 h_2}{\theta_2}\right)(\Delta U_{12} - \Delta U_{13}) + \frac{1}{2\rho_3 T_3}\left(\frac{1}{\sigma_3}\frac{\rho_3 h_3}{\theta_3}\right)[d_{13}\Delta U_{13} + d_{23}(\Delta U_{13} - \Delta U_{12})] . \tag{B.44}$$

- $r_{gP}(W) =$

$$r_{gP_1} = -\frac{1}{\rho_2 T_2}\left(\frac{G_{22}}{\sigma_2} - \frac{\rho_2 h_2 F_{22}}{\theta_2 T_2}\right) + \frac{1}{\rho_3 T_3}\left(\frac{G_{23}}{\sigma_3} - \frac{\rho_3 h_3 F_{23}}{\theta_3 T_3}\right) , \tag{B.45}$$

$$r_{gP_2} = -\frac{1}{\rho_2 T_2}\left(\frac{G_{32}}{\sigma_2} - \frac{\rho_2 h_2 F_{32}}{\theta_2 T_2}\right) + \frac{1}{\rho_3 T_3}\left(\frac{G_{33}}{\sigma_3} - \frac{\rho_3 h_3 F_{33}}{\theta_3 T_3}\right) . \tag{B.46}$$

- $r_{gT}(W) =$

$$r_{gT_1} = -\frac{1}{\rho_2 T_2}\left(\frac{1}{\sigma_2} - \frac{\rho_2 h_2}{\theta_2 T_2}\right)(q_{12} + q_{23}) - \frac{q_{23}}{\rho_3 T_3}\left(\frac{1}{\sigma_3} - \frac{\rho_3 h_3}{\theta_3 - T_3}\right) , \tag{B.47}$$

$$r_{gT_2} = \frac{q_{23}}{\rho_2 T_2}\left(\frac{1}{\sigma_2} - \frac{\rho_2 h_2}{\theta_2 T_2}\right) + \frac{1}{\rho_3 T_3}\left(\frac{1}{\sigma_3} - \frac{\rho_3 h_3}{\theta_3 T_3}\right)(q_{13} + q_{23}) . \tag{B.48}$$

- $r_g(W) =$

$$-\Lambda_{23}\left[\frac{1}{\rho_2 T_2}\left(\frac{h_2}{\sigma_2} - \frac{\rho_2 c_2^2}{\sigma_2}\left.\frac{\partial \epsilon_2}{\partial P_2}\right|_{\rho_2} - \frac{\rho_2 h_2}{\theta_2 T_2}\left(\epsilon_2 + \rho_2 \left.\frac{\partial \epsilon_2}{\partial \rho_2}\right|_{T_2}\right)\right) + \frac{1}{\rho_3 T_3}\left(\frac{h_3}{\sigma_3} - \frac{\rho_3 c_3^2}{\sigma_3}\left.\frac{\partial \epsilon_3}{\partial P_3}\right|_{\rho_3} - \frac{\rho_3 h_3}{\theta_3 T_3}\left(\epsilon_3 + \rho_3 \left.\frac{\partial \epsilon_3}{\partial \rho_3}\right|_{T_3}\right)\right)\right] \tag{B.49}$$

Appendix C. Velocity relaxation algorithm

The sub-system that characterizes this step can be written as follows:

$$\begin{cases} \partial_t \alpha_k = 0 \\ \partial_t m_k = 0 \\ \partial_t \left(m_k U_k\right) = -\sum_{l=1, l\neq k}^{3} d_{kl}(W)\Delta U_{kl} \\ \partial_t \left(\alpha_k E_k\right) = -\sum_{l=1, l\neq k}^{3} V_{kl}(W)\cdot d_{kl}(W)\Delta U_{kl} \end{cases} \tag{C.1}$$

From (C.1), one can obtain the following equation:

$$\partial_t \Delta U = -\widehat{R}_{UU} \Delta U, \tag{C.2}$$

with $\widehat{R}_{UU} \in M_2(\mathbb{R})$ that corresponds to the matrix R_{UU} of (B.2) with $\Delta g_{23} = 0$; The algorithm used for computing approximate solutions for the velocity relaxation step is identical to Algorithm 3.3.1.2 presented in [9]. It consists, on each cell of the mesh, in five steps:

Step 1. Initialize the vector of velocity differences at time t^{n-} (right after the convective step): $\Delta U^{n-} = (\Delta U_{12}^{n-}, \Delta U_{13}^{n-})^\intercal$ and matrix $\widehat{R}_{UU}$ at time t^{n-}.

Step 2. Compute ΔU^n such as:

$$\left(\mathcal{I} + \Delta t_n \widehat{R}_{UU}(W^{n-})\right) \Delta U^n = \Delta U^{n-} \ , \tag{C.3}$$

with $\mathcal{I}$ the identity matrix in $M_2(\mathbb{R})$.

Step 3. Compute U_1^n using the total momentum conservation:

$$U_1^n = \frac{\sum_{k=1}^3 (m_k \mathbf{U}_k)^{n-} + m_2^{n-} \Delta U_{12}^n + m_3^{n-} \Delta U_{13}^n}{(m_1 + m_2 + m_3)^{n-}} \ . \tag{C.4}$$

Step 4. Update U_2^n and U_3^n as:

$$U_2^n = U_1^n - \Delta U_{12}^n \quad ; \quad U_3^n = U_1^n - \Delta U_{13}^n \ . \tag{C.5}$$

Step 5. Update the total energy by integrating the evolution equation of the total energy of system (C.1):

$$(\alpha_k E_k)^n = (\alpha_k E_k)^{n-} - \Delta t \sum_{l=1, l\neq k}^{3} \frac{d_{kl}\,(W^{n-})}{2} \left((U_k^n)^2 - (U_l^n)^2\right) \tag{C.6}$$

Appendix D. Interfacial area

The definition of an interfacial area $\mathcal{A}_1$ for the phase 1 (corium) is needed in order to capture the behaviour of the solution [5, 13, 25]:

$$\mathcal{A}_1 = \frac{6\alpha_1}{D_1} \tag{D.1}$$

Its equation of evolution is supposed to be:

$$\frac{\partial \mathcal{A}_1}{\partial t} + \nabla(\mathcal{A}_1 U_1) = g(\mathcal{A}_1, W); \tag{D.2}$$

with, see [8, 52]:

$$g(\mathcal{A}_1, W) = C_0 \frac{\mathcal{A}_1^2}{6\alpha_1} \left(\frac{\rho_1}{\rho_2}\right)^{1/2} \|U_1 - U_2\| f(We); \tag{D.3}$$

where the coefficient $C_0 = 0.245$ and We the Weber number is defined as follows:

$$We = \frac{\rho_1 \|U_1 - U_2\|^2 D_1}{\sigma_1} \tag{D.4}$$

with $\sigma_1 = 73\ .10^{-3}(\mathrm{N.m^{-1}})$ a reference surface tension [51]. Moreover $f(We)$ is defined as:

$$f(We) = 1 \ , \ if \ \ We > We_c \ ; \ f(We) = 0 \text{ otherwise} \tag{D.5}$$

where $We_c = 12$ is called the critical Weber number.

Adding this new equation does not change the structure and properties of the global system (1.4) according to [8]. Hence, it is chosen for the simulation. The numerical scheme used to simulate (D.2) is detailed in [8]. It consists of an explicit implicit step method, splitting the convective part and the source term part. Those two steps will respectively be inserted inside the explicit simulation step of the convective part of system (1.4) and the implicit simulation of the source terms of the same system.

References

[1] Annalisa Ambroso, Christophe Chalons, and Pierre-Arnaud Raviart. A Godunov-type method for the seven-equation model of compressible two-phase flow. *Comput. Fluids*, 54:67–91, 2012.

[2] Bruno Audebert. *Contribution à l'analyse des modèles aux tensions de Reynolds pour l'interaction choc turbulence*. PhD thesis, Université Pierre et Marie Curie - Paris VI, 2006. `https://theses.hal.science/tel-00850928`.

[3] Melvin R. Baer and Jace W. Nunziato. A two phase mixture theory for the deflagration to detonation transition (DDT) in reactive granular materials. *Int. J. Multiphase Flow*, 12-6:861–889, 1986.

[4] Christophe Berthon, Frédéric Coquel, Jean-Marc Hérard, and Markus Uhlmann. An approximate solution of the Riemann problem for a realisable second-moment turbulent closure. *Shock Waves*, 11(4):245–269, 2002.

[5] Georges Berthoud. Vapor Explosions. *Ann. Rev. Fluid Mech.*, 32(1):573–611, 2000.

[6] Zbigniew Bilicki and Joseph Kestin. Physical aspects of the relaxation model in two-phase flow. *Proc. R. Soc. Lond., Ser. A*, 428(1875):379–397, 1990.

[7] Sebastiano Boscarino and Giovanni Russo. Asymptotic preserving methods for quasilinear hyperbolic systems with stiff relaxation: a review. *SeMA J.*, 81(1):3–49, 2024.

[8] Hamza Boukili and Jean-Marc Hérard. Relaxation and simulation of a barotropic three-phase flow model. *ESAIM, Math. Model. Numer. Anal.*, 53:1031–1059, 2019.

[9] Hamza Boukili and Jean-Marc Hérard. Simulation and preliminary validation of a three-phase flow model with energy. *Comput. Fluids*, 221: article no. 104868, 2021.

[10] Didier Bresch and Matthieu Hillairet. A compressible multifluid system with new physical relaxation terms. *Ann. Sci. Éc. Norm. Supér.*, 52:255–295, 2019.

[11] Jean Bussac. Study of relaxation processes in a two-phase flow model. *ESAIM, Proc. Surv.*, 72:2–18, 2023.

[12] John Charles Butcher. *Numerical methods for ordinary differential equations*. John Wiley & Sons, 2016.

[13] Alice Chauvin, Eric Daniel, Ashwin Chinnayya, Jacques Massoni, and Georges Jourdan. Shock waves in sprays: numerical study of secondary atomization and experimental comparison. *Shock Waves*, 26:403–415, 2016.

[14] Simone Chiocchetti and Christoph Müller. A Solver for Stiff Finite-Rate Relaxation in Baer–Nunziato Two-Phase Flow Models. In Grazia Lamanna, Simona Tonini, Gianpietro Elvio Cossali, and Bernhard Weigand, editors, *Droplet Interactions and Spray Processes*, pages 31–44. Springer, 2020.

[15] Frédéric Coquel, Thierry Gallouët, Jean-Marc Hérard, and Nicolas Seguin. Closure laws for a two fluid two-pressure model. *C. R. Acad. Sci. Paris*, I-332:927–932, 2002.

[16] Frédéric Coquel, Jean-Marc Hérard, and Khaled Saleh. A positive and entropy-satisfying finite volume scheme for the Baer–Nunziato model. *J. Comput. Phys.*, 330:401–435, 2017.

[17] Fabien Crouzet, Frédéric Daude, Pascal Galon, Jean-Marc Hérard, Olivier Hurisse, and Yujie Liu. Validation of a two-fluid model on unsteady liquid-vapor water flows. *Comput. Fluids*, 119:131–142, 2015.

[18] Gianni Dal Maso, Philippe G. Le Floch, and François Murat. Definition and weak stability of nonconservative products. *J. Math. Pures Appl.*, 74(2):483–548, 1995.

[19] Davide Ferrari, Ilya Peshkov, Evgeniy Romenski, and Michael Dumbser. A unified SHTC multiphase model of continuum mechanics. https://arxiv.org/abs/2403.19298, 2024.

[20] Tore Flåtten and Gaute Linga. A hierarchy of non-equilibrium two-phase flow models. *ESAIM, Proc. Surv.*, 66:109–143, 2019.

[21] Tore Flåtten and Halvor Lund. Relaxation two-phase flow models and the sub-characteristic condition. *Math. Models Methods Appl. Sci.*, 21:2379–2407, 2011.

[22] Thierry Gallouët, Jean-Marc Hérard, and Nicolas Seguin. Numerical modeling of two-phase flows using the two fluid two-pressure approach. *Math. Models Methods Appl. Sci.*, 14:663–700, 2004.

[23] Sergey Gavrilyuk. The structure of pressure relaxation terms: the one-velocity case, 2014. EDF report H-I83-2014-0276-EN. Available upon request to: sergey.gavrilyukuniv-amu.fr.

[24] Sergey Gavrilyuk and Richard Saurel. Mathematical and numerical modeling of two-phase compressible flows with micro-inertia. *J. Comput. Phys.*, 175:326–360, 2002.

[25] Boris E. Gelfand. Droplet breakup phenomena in flows with velocity lag. *Prog. Energy Combust. Sci.*, 22(3):201–265, 1996.

[26] James Glimm, David Saltz, and David H. Sharp. Two phase flow modelling of a fluid mixing layer. *J. Fluid Mech.*, 378:39–47, 1999.

[27] Lene Grabowsky, Maren Hantke, and Siegfried Müller. News on Baer–Nunziato type model at pressure equilibrium. *Contin. Mech. Thermodyn.*, 33:767–788, 2021.

[28] Vincent Guillemaud. *Modelisation et simulation numerique des ecoulements diphasiques par une approche bifluide a deux pressions*. PhD thesis, Université Aix-Marseille, 2007. Available at : https://tel.archives-ouvertes.fr/tel-00169178v1.

[29] Maren Hantke, Siegfried Muller, Aleskey Sikstel, and Ferdinand Thein. Baer–Nunziato type models for isothermal and isentropic flows. to appear in *ESAIM, Proc. Surv.*, 2025.

[30] Jean-Marc Hérard. A three-phase flow model. *Mathematical and Computer Modeling*, 45:732–755, 2007.

[31] Jean-Marc Hérard. Une classe de modèles diphasiques bifluides avec changement de régime, 2012. internal EDF report H-I81-2010-0486-FR, in French. An abridged version of this note is published on AIAA paper 2012-3356 and available at https://hal.archives-ouvertes.fr/hal-01582645/file/aiaa2012_3356.pdf.

[32] Jean-Marc Hérard. A class of three-phase flow models with energy, 2020. internal EDF report 6125-3016-2020-01853-EN.

[33] Jean-Marc Hérard and Olivier Hurisse. A fractional step method to compute a class of compressible gas-liquid flows. *Comput. Fluids*, 55:57–69, 2012.

[34] Jean-Marc Hérard, Olivier Hurisse, and Lucie Quibel. A four-field three-phase flow model with both miscible and immiscible components. *ESAIM, Math. Model. Numer. Anal.*, 55:S251–S278, 2021.

[35] Jean-Marc Hérard and Guillaume Jomée. Two approaches to compute unsteady compressible two-phase flow models with stiff relaxation terms. *ESAIM, Math. Model. Numer. Anal.*, 57(6):3537–3583, 2023.

[36] Jean-Marc Hérard and Guillaume Jomée. Relaxation process in a hybrid two-phase flow model, 2025. in revision, https://hal.science/hal-04197280v2.

[37] Jean-Marc Hérard and Yujie Liu. Une approche bifluide statistique de modélisation des écoulements diphasiques à phases compressibles. EDF report H-I81-2013-01162-FR, https://hal.science/hal-03092682.

[38] Jean-Marc Hérard and Hélène Mathis. A three-phase flow model with two miscible phases. *ESAIM, Math. Model. Numer. Anal.*, 53:1373–1389, 2019.

[39] I. Huhtiniemi, H. Hohmann, R. Faraoni, M. Field, R. Gambaretti, and K. Klein. KROTOS 38 to KROTOS 44: data report, 1996. IRSN Technical Note No. I.

[40] Mamoru Ishii. Thermo-fluid dynamic theory of two-phase flow, 1975. Eyrolles-Collection de la Direction des Etudes et Recherches EDF.

[41] Guillaume Jomée. *Simulation of compressible non-equilibrium multiphase flow models*. PhD thesis, Aix-Marseile Université, 2023. `https://hal.science/tel-04338786`.

[42] Ashwani Kapila, Steven F. Son, John B. Bdzil, Ralph Menikoff, and Donald S. Stewart. Two phase modeling of a DDT: structure of the velocity relaxation zone. *Phys. Fluids*, 9-12:3885–3897, 1997.

[43] Tosio Kato. The Cauchy problem for quasi-linear symetric hyperbolic systems. *Arch. Ration. Mech. Anal.*, 58:181–205, 1975.

[44] Halvor Lund. A Hierarchy of Relaxation Models for Two-Phase Flow. *SIAM J. Appl. Math.*, 72:1713–1741, 2012.

[45] Maxima. Maxima : A Computer Algebra System. `https://maxima.sourceforge.io/`.

[46] Renaud Meignen, Bruno Raverdy, Stéphane Picchi, and Julien Lamome. The challenge of modeling fuel–coolant interaction: Part II–Steam explosion. *Nucl. Eng. Des.*, 280:528–541, 2014.

[47] Siegfried Müller, Maren Hantke, and Pascal Richter. Closure conditions for non-equilibrium multi-component models. *Contin. Mech. Thermodyn.*, 28:1157–1189, 2016.

[48] Marica Pelanti. Arbitrary-rate relaxation techniques for the numerical modeling of compressible two-phase flows with heat and mass transfer. *Int. J. Multiphase Flow*, 153: article no. 104097, 2022.

[49] Marica Pelanti and Keh-Ming Shyue. A numerical model for multiphase liquid–vapor–gas flows with interfaces and cavitation. *Int. J. Multiphase Flow*, 113:208–230, 2019.

[50] Vincent Perrier and Enrique Gutiérrez. Derivation and closure of Baer and Nunziato type multiphase models by averaging a simple stochastic model. *Multiscale Model. Simul.*, 19(1):401–439, 2021.

[51] Stéphane Picchi. *MC3D Version 3.9 : Description of the models of the premixing application*. IRSN internal report, 2017.

[52] Martin M. Pilch and CA Erdman. Use of breakup time data and velocity history data to predict the maximum size of stable fragments for acceleration-induced breakup of a liquid drop. *Int. J. Multiphase Flow*, 13(6):741–757, 1987.

[53] Pratik Rai. *Modeling and numerical simulation of compressible multicomponent flows*. PhD thesis, Institut Polytechnique de Paris, 2021. Available at : `https://tel.archives-ouvertes.fr/tel-03461287`.

[54] William E. Ranz. Evaporation from Drops-I and-II. *Chem. Eng. Progr*, 48:141–146, 1952.

[55] Khaled Saleh. A relaxation scheme for a hyperbolic multiphase flow model-Part I: Barotropic EOS. *ESAIM, Math. Model. Numer. Anal.*, 53(5):1763–1795, 2019.

[56] Donald W. Schwendeman, Christopher W. Wahle, and Ashwana K. Kapila. The Riemann problem and a high-resolution Godunov method for a model of compressible two-phase flow. *J. Comput. Phys.*, 212(2):490–526, 2006.

[57] Mai D. Thanh, Dietmar Kröner, and Nguyen T. Nam. Numerical approximation for a Baer–Nunziato model of two-phase flows. *Appl. Numer. Math.*, 61(5):702–721, 2011.

[58] Svetlana A. Tokareva and Eleuterio F. Toro. HLLC-type Riemann solver for the Baer–Nunziato equations of compressible two-phase flow. *J. Comput. Phys.*, 229(10):3573–3604, 2010.

[59] Gerhard Wanner and Ernst Hairer. *Solving ordinary differential equations. II: Stiff and differential-algebraic problems*, volume 14 of *Springer Series in Computational Mathematics*. Springer, 1996.

[60] Linkai Wei. *Development of a new steam explosion model for the MC3D software*. Theses, Université de Lorraine, 2023. `https://theses.hal.science/tel-04216777`.